JOURNAL OF PETROLOGY | VOLUME 51 | NUMBERS 1 & 2 | PAGES 513–535 | 2010 | doi:10.1093/petrology/egp091

Eclogites and Garnet Pyroxenites: Problems Resolving Provenance Using Lu–Hf, Sm–Nd and Rb–Sr Isotope Systems

R. G. GONZAGA[1]*, M. A. MENZIES[1], M. F. THIRLWALL[1], D. E. JACOB[2] AND A. LEROEX[3]

[1]DEPARTMENT OF EARTH SCIENCES, ROYAL HOLLOWAY UNIVERSITY OF LONDON, EGHAM TW20 0EX, UK

[2]INSTITUT FÜR GEOWISSENSCHAFTEN, UNIVERSITÄT MAINZ, BECHERWEG 21, D-55099 MAINZ, GERMANY

[3]DEPARTMENT OF GEOLOGICAL SCIENCES, UNIVERSITY OF CAPE TOWN, RONDEBOSCH, 7701, SOUTH AFRICA

RECEIVED DECEMBER 29, 2008; ACCEPTED NOVEMBER 27, 2009
ADVANCE ACCESS PUBLICATION JANUARY 6, 2010

Cratonic eclogites and garnet pyroxenites from the Kaapvaal craton have heterogeneous Hf–Nd–Sr–(O) isotope ratios that define a positive Hf–Nd isotope array and a negative Nd–Sr isotope array. Isotopic variability encompasses depleted (mid-ocean ridge basalt and ocean-island basalt) to enriched mantle compositions (Group I and II kimberlites) and overlaps with that of the Kaapvaal craton garnet peridotite xenoliths. Isotopic heterogeneity at Roberts Victor is less extreme than previously reported and ranges from eclogites with a highly depleted MORB-like signature to enriched eclogites similar to Group II and transitional kimberlites and Group II megacrysts ($\varepsilon_{Hf} = -32{\cdot}8$). Much of this similarity may well be due to partial or complete resetting during entrainment. For the majority of eclogites and garnet pyroxenites the Lu–Hf system records 'older' mantle events than the Sm–Nd system, but neither necessarily records the protolith age. Both the Lu–Hf and the Sm–Nd systems are prone to being reset by entrainment in high-temperature kimberlite and/or basaltic magmas (e.g. Kaapvaal) and emplacement in orogenic belts (e.g. Beni Bousera). In the case of one eclogite from Roberts Victor the Sm–Nd cpx–gt mineral isochron age (963·1 ± 42·3 Ma) differs from the Lu–Hf cpx–gt mineral isochron age (1953 ± 13 Ma) by 1 Ga and the Rb–Sr clinopyroxene model age (3·15 Ga) is 1 Ga older than the Lu–Hf age and the reconstructed whole-rock isochron age. Ironically, it may be that, in this instance, the Rb–Sr system gives a better indication of protolith age than Sm–Nd or Lu–Hf. Overall variable resetting of isotope systems between protolith formation in the Archaean (>2·5 Ga) and kimberlite and/or basalt entrainment (≤0·2 Ga) masks our understanding of the exact protolith age of eclogites.

KEY WORDS: *cratonic eclogite; garnet pyroxenite; Kaapvaal; Lu–Hf; Sm–Nd isotopes*

INTRODUCTION

Eclogites occur primarily within continents as tectonically emplaced bodies incorporated into orogenic belts (<2·5 Ga) or as kimberlite-hosted high-pressure xenoliths in cratons (>2·5 Ga). Over the last hundred years the origin of eclogites has been variably attributed to crustal magmatic processes and recycling of basaltic protoliths (e.g. MacGregor & Manton, 1986). Garnet pyroxenites are more widespread, being found in both oceanic and continental (cratonic and circum-cratonic) environments. High-pressure polybaric fractionation of mafic or ultramafic magmas in the mantle (e.g. Irving, 1980) has been the favoured model for their genesis. Recently models involving peridotitic mantle source regions for oceanic magmas have been challenged with the proposal that olivine-free pyroxenites have a vital role to play in their genesis (Hirshmann & Stolper, 1996; Sobolev *et al.*, 2005). As a consequence constraints are needed on the provenance (age and origin) of garnet–pyroxene assemblages (eclogites and garnet pyroxenites) formed at mantle pressures and temperatures.

Over the last 10 years eclogites (omphacitic pyroxene + pyropic garnet) and garnet pyroxenites (majoritic? pyroxene + pyropic garnet) have been studied for their

*Corresponding author. Telephone: 00 (44) 7814 681447.
E-mail: gonzagarg@yahoo.com.br

Lu–Hf and Sm–Nd isotope systematics from both orogenic belts and basalt- and kimberlite-hosted xenolith suites. Orogenic eclogite isotopic data are available from the Himalayas, India (de Sigoyer *et al.*, 2000), the Franciscan Coastal Ranges, California (Anczkiewicz *et al.*, 2004), the Alpine Orogen of Morocco (Blichert-Toft *et al.*, 1999; Pearson & Nowell, 2004), the Caledonides of Norway (Lapen *et al.*, 2005) and the Dabie Orogen, China (Cheng *et al.*, 2008). Eclogite and garnet pyroxenite xenoliths hosted in mantle-derived mafic magmas have been studied for Sr–Nd–Hf–Pb isotopes, mainly from the Bearpaws Mountains, USA (Scherer *et al.*, 2000), Malaita (Ishikawa *et al.*, 2007) and Hawaii (Bizimis *et al.*, 2005). Kimberlite-hosted elogites have been studied for Sr–Nd–Pb–O isotopes and, more recently, combined Sm–Nd and Lu–Hf isotopes. Much of this work has focused on the Roberts Victor eclogites (Jacob *et al.*, 2005; Gonzaga, 2007) because of the scarcity of eclogites in most other cratonic kimberlite pipes.

Clinopyroxene–garnet mineral ages have been calculated to constrain the age and origin of the protolith. In some cases the Lu–Hf and Sm–Nd mineral isochron ages record similar 'events' (Pearson & Nowell, 2004; Ishikawa *et al.*, 2007) but in others the Lu–Hf and Sm–Nd mineral isochron ages can differ significantly (Jacob *et al.*, 2005; Lapen *et al.*, 2005; Gonzaga, 2007). Where ages are similar, the Lu–Hf and Sm–Nd clinopyroxene–garnet mineral ages may record (1) their formation in the upper mantle (Lapen *et al.*, 2005), or (2) thermo-tectonic processes that have partially or completely reset the isotope systems (Cheng *et al.*, 2008), including entrainment during crack propagation and magma transfer (Jacob *et al.*, 2005; Ishikawa *et al.*, 2007) or polybaric emplacement from mantle P–T (Anczkiewicz *et al.*, 2004; Pearson & Nowell, 2004; Cheng *et al.*, 2008). For example, for the Beni Bousera diamondifereous garnet pyroxenites the Lu–Hf and Sm–Nd ages are identical to the emplacement–exhumation age determined for the orogenic peridotite massif using other approaches (Pearson & Nowell, 2004). Similarly in the case of Malaita, it has been suggested that the Sm–Nd and Lu–Hf ages are a proxy for the age of the intrusion of the host alnöitic magma (Ishikawa *et al.*, 2007). However, where protolith ages are older than entrainment or emplacement ages (Scherer *et al.*, 2000; Jacob *et al.*, 2005; Lapen *et al.*, 2005; Gonzaga, 2007) the Lu–Hf age is frequently taken as a measure of the original protolith age.

For this study, eclogite and garnet pyroxenite xenoliths from Roberts Victor, Lovedale, Bultfontein and Roodekraal in the Kaapvaal craton (Fig. 1) were analysed for Lu–Hf, Sm–Nd and Rb–Sr isotopes. These samples are hosted in Mesozoic kimberlites and associated alkaline rocks in southern Africa; namely, Group II kimberlites (120–150 Ma) and Group I kimberlites (80–95 Ma) of Smith (1983). Additionally, a garnet clinopyroxenite from Malaita, Solomon Islands, was included for comparison. Mineral, trace element and oxygen isotope data for these samples have been reported by Gonzaga *et al.* (2009). The aims of this study are:

(1) to present new Lu–Hf and Sm–Nd isotopic data for cratonic eclogites and garnet pyroxenites from Kaapvaal;
(2) to compare Sm–Nd and Lu–Hf clinopyroxene–garnet mineral isochrons in an evaluation of the extent to which they can be used to establish the protolith 'age';
(3) to assess the extent to which these isotope data are useful in evaluating the role eclogites and garnet pyroxenites can play in oceanic magmatism.

ANALYTICAL TECHNIQUE

In an attempt to minimize the effects of artefacts introduced by infiltration of the kimberlite–alnöite host magma and subsequent alteration (e.g. Jacob *et al.*, 2005), analyses of Sm–Nd and Lu–Hf were carried out only on garnet and clinopyroxene mineral separates rather than whole-rock powders. Sr isotope determinations were performed on clinopyroxene as this fraction contains the bulk of the Sr in the rock and has a low Rb/Sr such that the measured isotope ratio is close to the initial value. Rock chips were crushed in a steel mortar and sieved to fractions between 500–250 μm and 250–150 μm, rinsed, ultrasonicated and dried in an oven. Optically clear mineral fragments were hand picked under a binocular microscope. Chemical separation and spiking for Sm, Nd, Lu and Hf generally follow the approach of Anczkiewicz & Thirlwall (2003), with some adjustments and modifications as described below.

Some of the garnet fractions were separated for use in the H_2SO_4 leaching protocol proposed by Anczkiewicz & Thirlwall (2003). However, it became clear that the leaching procedures did not produce different elemental ratio or isotope ratio data, so most samples were not leached. All samples were spiked with ^{149}Sm–^{150}Nd and ^{176}Lu–^{180}Hf solutions. The spike mass required for near-optimal spiking was estimated from elemental concentration data for each sample measured by laser ablation inductively coupled plasma mass spectrometry (LA-ICPMS). The low Sm/Nd ratios in clinopyroxene required the use of a mixed ^{149}Sm–^{150}Nd spike with lower Sm/Nd ratio. For analyses of Lu and Hf, the available mixed spike was not well suited to the very low Lu/Hf ratios (often less than 0·040) in our clinopyroxenes. To avoid overspiking of Lu, additional diluted ^{180}Hf spike was added to this fraction. This use of separate Lu/Hf and Hf spikes for clinopyroxenes means that we lose the accuracy advantage of the mixed spike. This is not a significant problem for clinopyroxenes in this study, as their Lu/Hf ratios are so low that

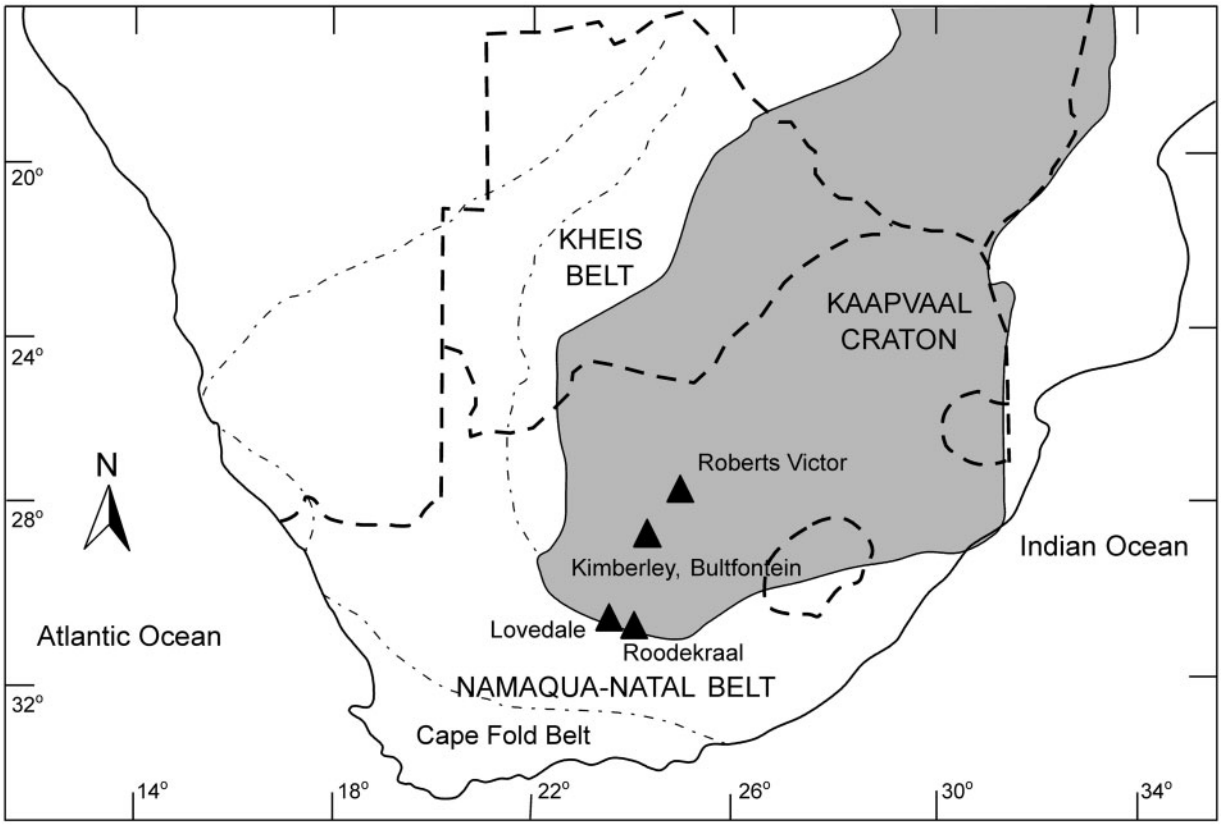

Fig. 1. Location of the southern African samples (Kimberley, Roberts Victor, Bultfontein, Lovedale and Roodekraal pipes). Geographical co-ordinates are given in Table 2.

even several per cent uncertainty would not worsen the error on Lu–Hf ages.

Elemental separation was undertaken in four column steps [details have been given by Anczkiewicz & Thirlwall (2003)]: (1) separation of high field strength elements (HFSE), Lu and other rare earth elements (REE) on a BioRad AG 50W-X8 cation resin column followed by a second pass for purification of the HFSE separate; (2) separation of Hf from other HFSE on an Eichrom® Ln-Spec resin filled column (LN); (3) separation of Nd and Sm from other REE on larger Ln-Spec columns; (4) purification of the Lu separate from Ba, Gd, Tb, Dy and Yb on the same Ln-Spec columns as used for Nd. Total procedure blanks were ~170 pg for Nd and 5–10 pg for Hf. The Hf blank is insignificant relative to minimum analyte masses of 10·8 ng. The Nd blank represents <1·3% of the analyte Nd.

For samples from Bultfontein, Roodekraal and Lovedale, a Sr fraction was also taken from the first cation columns and was further purified using Eichrom® Sr-spec resin prior to thermal ionization mass spectrometry (TIMS) analysis. Analyses of Sr isotopic ratios for samples from Malaita and Roberts Victor were performed on different clinopyroxene separates, as they occurred after the analyses of Hf and Nd. The Sr separates were loaded using H_3PO_4 on Re single filaments previously degassed at 5·2 A for TIMS analyses.

Multicollector (MC)-ICP-MS analyses were carried out in static mode on the Royal Holloway GV Instruments IsoProbe using the approach of Thirlwall & Anczkiewicz (2004). Static mode was used because of the relatively low analyte masses; however, this carries a penalty in poorer reproducibility of standards than in multidynamic analysis as discussed in detail by Thirlwall & Anczkiewicz (2004). This includes systematic changes in standard ratios during a day and between-day differences that are not present in multidynamic data obtained simultaneously (Thirlwall & Anczkiewicz, 2004). This poorer reproducibility does not matter for Lu and Sm analysis as reproducibility of static $^{176}Lu/^{175}Lu$ and $^{147}Sm/^{149}Sm$ in unspiked standards is <0·1% 2SD. Correction for these effects is, however, critical in Nd and Hf isotope analysis. To minimize the effects of secular drift in static ratios, samples used for isochron determinations were analysed in consecutive runs, and standards were run every 2–3 samples. Further, Vance & Thirlwall (2002) and Thirlwall & Anczkiewicz (2004)

Table 1: Analyses of the Nd (Aldrich), Hf (JMC475) and Sr (SRM987) standards over time

	Nd (Aldrich)								
	$^{142}Nd/^{144}Nd$	2SD	$^{143}Nd/^{144}Nd$	2SD	$^{145}Nd/^{144}Nd$	2SD	$^{150}Nd/^{144}Nd$	2SD	*N*
22,23-Nov-04	1·14162	0·00008	0·511357	0·000010	0·348399	0·000017	0·236295	0·000058	11
10,12-Jan-07	*	*	0·511420*	0·000013	0·348482*	0·000017	0·236351*	0·000019	16
TIMS	1·141877	0·000015	0·511413	0·000008	0·348408	0·000005	0·236491	0·000010	~8
IsoProbe	1·14152	0·00006	0·511354	0·000015	0·348417	0·000010	0·236371	0·000019	29
	Hf (JMC475)								
	$^{174}Hf/^{177}Hf$	2SD	$^{176}Hf/^{177}Hf$	2SD	$^{178}Hf/^{177}Hf$	2SD	$^{180}Hf/^{177}Hf$	2SD	*N*
06-Feb-04	0·008657	0·000001	0·282197	0·000018†	1·46732	0·00004	1·88679	0·00008	4
24,27-Jan-05	0·008659	0·000009	0·282157	0·000026†	1·46732	0·00009	1·88677	0·00010	10
04-Apr-06	0·008658	0·000003	0·282177	0·000013	1·46727	0·00004	1·88679	0·00008	6
26-Jan-07	0·008657	0·000003	0·282165	0·000010	1·46730	0·00003	1·88672	0·00007	7
IsoProbe	0·008659	0·000005	0·282165	0·000018	1·46733	0·00009	1·88686	0·00014	88
	Sr (SRM987)								
	$^{87}Sr/^{86}Sr$	2SD	*N*						
10-Oct-06	0·710245	0·000008	10						

*Data corrected to $^{142}Nd/^{144}Nd = 1·14187$ according to Thirlwall & Anczkiewicz (2004).
†Relatively poor external precision reflects secular drift in $^{176}Hf/^{177}Hf$.
Nd data normalized to $^{146}Nd/^{144}Nd = 0·7219$. Hf data normalized to $^{179}Hf/^{177}Hf = 0·7325$. *N*, number of ratios.
TIMS and IsoProbe (pre-upgrade to high-sensitivity interface pumping option) multidynamic reference data from Thirlwall & Anczkiewicz (2004).

showed correlations between exponential-law-normalized $^{142}Nd/^{144}Nd$ and $^{143}Nd/^{144}Nd$ of our Aldrich Nd standard in both static and multidynamic runs on the IsoProbe. They also showed that the gradient of these correlations is similar to multidynamic TIMS data and to data from Nu Plasma and P54 MC-ICP-MS instruments elsewhere. Correction of multidynamic IsoProbe data to constant $^{142}Nd/^{144}Nd$ yielded highly reproducible $^{143}Nd/^{144}Nd$ standard data, identical to multidynamic TIMS data. Vance & Thirlwall (2002) also demonstrated that applying such corrections to the La Jolla Nd standard and to Nd from a Hawaiian sediment sample yielded similar reproducibility to TIMS, and also gave accurate data. These correlations were attributed to a varying component of non-exponential mass bias on the IsoProbe. Static $^{143}Nd/^{144}Nd$ standard data in general need a correction for the offset from the multidynamic ratio, as well as the correction to constant $^{142}Nd/^{144}Nd$.

Nd isotopic analyses in this study were determined on two separate occasions in November 2004 and January 2007. The first used soft extraction and yielded very reproducible Nd ratios for our Aldrich standard (±0·000010 2SD for $^{143}Nd/^{144}Nd$, Table 1). Measured sample $^{143}Nd/^{144}Nd$ were corrected for the 0·000056 offset between the measured and TIMS values for Aldrich. The second occasion took place after installation of a high-sensitivity interface pumping option, which has the effect of producing relatively large variations in non-exponential mass bias. Tight correlations were observed between standard $^{142}Nd/^{144}Nd$ and $^{143}Nd/^{144}Nd$, $^{145}Nd/^{144}Nd$ and $^{150}Nd/^{144}Nd$ (MSWD of 1·3, 4·3 and 5·9 respectively), with the $^{143}Nd/^{144}Nd$–$^{142}Nd/^{144}Nd$ gradient (+0·317 ± 0·024, 2σ) within error of the multidynamic gradient reported by Thirlwall & Anczkiewicz (2004). Sample Nd isotope ratios were corrected using these observed gradients, and corrected standard data are reported in Table 1.

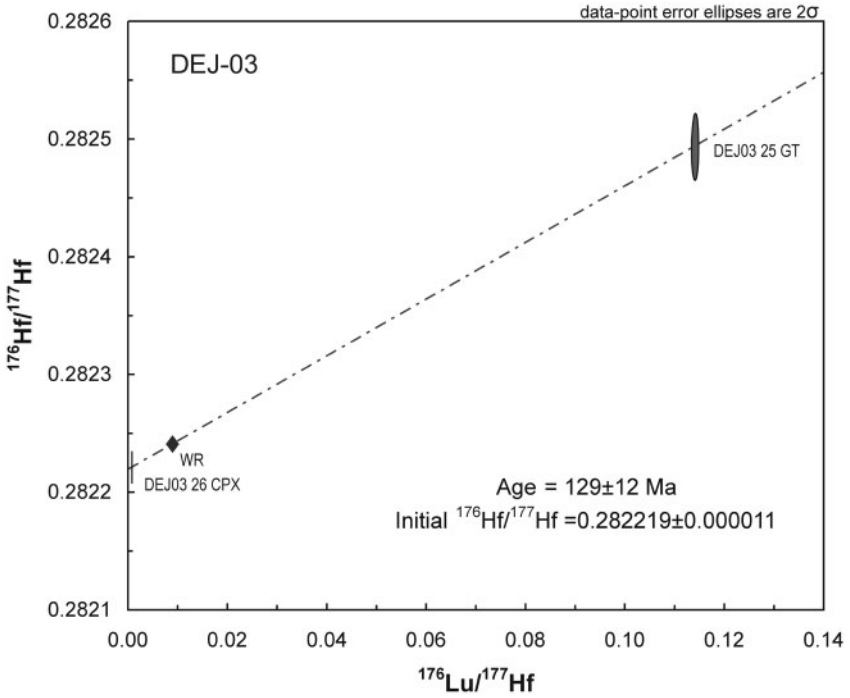

Fig. 2. Lu–Hf clinopyroxene–garnet isochron for sample DEJ03 from Roberts Victors, reset at the time of kimberlite emplacement (127 Ma).

The reproducibility of standard $^{143}Nd/^{144}Nd$ (±0·000013, 2SD) is of course substantially enhanced relative to the uncorrected measurements; we take this uncertainty as the minimum sample uncertainty based on the experiments with La Jolla and the Hawaiian sediment sample by Vance & Thirlwall (2002).

Hf isotope analyses were performed on four separate occasions between 2004 and 2007. On the two later occasions JMC475 static $^{176}Hf/^{177}Hf$ results were reproducible to ≤±0·000013 (2SD, Table 1), and sample $^{176}Hf/^{177}Hf$ data have been corrected for the offset from 0·282165 for JMC475 if necessary. The two earlier occasions formed part of longer periods when static $^{176}Hf/^{177}Hf$ in JMC475 increased systematically with time (see fig. 2 of Thirlwall & Anczkiewicz, 2004), and the $^{176}Hf/^{177}Hf$ reproducibility reported in Table 1 simply reflects the period over which analyses were determined and the rate of change of static ratios with time. Static JMC475 $^{176}Hf/^{177}Hf$ showed an overall increase from 0·28217 ± 1 on 23–26 January 2004 to 0·28220 ± 1 on 9 February 2004. From 24 to 27 January 2005, static $^{176}Hf/^{177}Hf$ increased from 0·282145 to 0·282172. Sample $^{176}Hf/^{177}Hf$ data for these periods were corrected by interpolation of the secular change in measured JMC475 $^{176}Hf/^{177}Hf$. The secular correlation has a width of about 0·000015 $^{176}Hf/^{177}Hf$ units, suggesting that overall reproducibility of the corrected data is about ±0·000010 2SD, similar to or better than most sample internal errors.

Sr was determined by TIMS on the Royal Holloway VG354 system using multidynamic methods (Thirlwall, 1991). Samples and standard SRM987 were loaded on Ta single filaments using H_3PO_4. Thirlwall (1991) reported reproducibility of multidynamic $^{87}Sr/^{86}Sr$ measurements at ±0·000014 (2SD) for more than 200 runs. The mean $^{87}Sr/^{86}Sr$ value for the 10 SRM987 standards run was 0·710245 ± 0·000008 (2SD).

Isochrons were calculated using the regression algorithm of York (1969) and error propagation of Titterington & Halliday (1979). Lu–Hf ages were calculated using the $1{\cdot}865 \pm 0{\cdot}015 \times 10^{-11}$ decay constant of Scherer *et al.* (2001) as supported by Soderlund *et al.* (2004).

DATA

The samples from Kaapvaal and Malaita are variably metasomatized (i.e. containing mica) and primarily composed of garnet and clinopyroxene (mode 40:60 to 60:40), with occasional orthopyroxene and accessory oxides and sulphides on the grain boundaries. The garnets are homogeneous pyrope and the clinopyroxenes show some retrograde petrographic and chemical change presumably caused by syn- or post-entrainment reaction with the host kimberlite (Table 2).

Elemental and isotopic data are presented in Table 3. Garnet initial ratios are in the range of $^{176}Hf/^{177}Hf =$ 0·281782–0·303013 and $^{143}Nd/^{144}Nd = 0{\cdot}512357$–0·516047

Table 2: Composition of pyroxenes and corresponding classification of samples (adapted from Gonzaga et al., 2009)

	Description	Pyroxene	Average mode	Accessories/alteration
Malaita (9°03′02·79″S, 160°58′13·13″E)				
RG01	garnet clinopyroxenite		55 gt:45 cpx:0 opx	opx, amphibole, sulphide
CPX	aluminian sodian	augite		
OPX	aluminian	enstatite		
Roodekraal (30°48′S, 24°13′E)				
RDK1	garnet clinopyroxenite		60 gt:40 cpx:0 opx	rutile, oxides
CPX core		omphacite		
CPX rim	aluminian sodian	diopside		
RDK2	garnet clinopyroxenite		75 gt:25 cpx:0 opx	mica
CPX	aluminian sodian	diopside		
OPX		enstatite		
Lovedale (30°34′S, 23°35′E)				
JAR 02073	eclogite		50 gt:50 cpx:0 opx	mica
CPX core		omphacite		
CPX rim	aluminian ferrian sodian	augite		
CPX rim	aluminian sodian	diopside		
JAR 02093	eclogite		40 gt:60 cpx:0 opx	carbonate, oxides
CPX core		omphacite		
CPX rim	aluminian sodian	augite		
Roberts Victor (28°29′38·4″S, 25°33′32·4″E)				
DEJ02	eclogite		65 gt:35 cpx:0 opx	
CPX core		omphacite		
CPX rim	aluminian sodian	augite		
DEJ03	eclogite		50 gt:50 cpx:0 opx	mica
CPX core		omphacite		
CPX rim	aluminian sodian	augite		
R30	garnet clinopyroxenite		50 gt:40 cpx:0 opx	amphibole, plagioclase
CPX	aluminian	augite		
CPX	aluminian sodian	diopside		
CPX	aluminian sodian	augite		
CPX	aluminian sodian	diopside		
CPX		omphacite		
Bultfontein (28°45′31·37″S, 24°49′1·02″E)				
713	garnet websterite		10 gt:70 cpx:15 opx	opaque minerals
CPX	aluminian chromian sodian	diopside		
CPX	chromian ferrian	augite		
CPX	chromian	augite		
OPX		enstatite		
OPX	ferrian	enstatite		
B21	garnet websterite		10 gt:75 cpx:10 opx	spinel
CPX	aluminian chromian sodian	augite		
CPX	chromian	aegirine–augite		
CPX	chromian	omphacite		
OPX		enstatite		

Accessory phases occur in the grain boundaries and as part of the alteration or secondary material within the intracrystalline spaces.

Table 3: Lu–Hf and Sm–Nd data for eclogites and garnet pyroxenites

	Malaita						
	RG01						
	GT	GT	GT	GT	GT	CPX	CPX
Batch	A	B	G	H1	H2	I	J
Hf ppm	0·956	0·900	0·949	0·950	0·956	0·835	1·014
Lu ppm	0·750	0·750	0·744	0·741	0·745	0·038	0·112
$^{176}Lu/^{177}Hf$	0·110791	0·11775	0·110718	0·110179	0·110169	0·006379	0·015549
2 SE	0·000554	0·000589	0·000554	0·000551	0·000551	0·000032	0·000078
$^{176}Hf/^{177}Hf$	0·283101	0·283093	0·28312	0·283069	0·283081	0·282956	0·282977
2 SE	0·000008	0·000015	0·000017	0·000021	0·000023	0·000016	0·000011
Batch			G		H2	I	J
Nd ppm			0·892947		0·907096	4·672703	6·956252
Sm ppm			1·013057		1·01724	1·568083	1·944018
$^{147}Sm/^{144}Nd$			0·685948		0·678036	0·202896	0·168964
2 SE			0·000686		0·000678	0·000203	0·000169
$^{143}Nd/^{144}Nd$			0·51296		0·512957	0·512852	0·512818
2 SE			0·000018		0·000016	0·000083	0·000015
$^{87}Sr/^{86}Sr$	0·703812						
2 SE	0·000013						
N	80						

	Roberts Victor								
	R30			DEJ03			DJ0288		
	GT		CPX	GT		CPX	GT	GT	CPX
Batch	23		24	25		26	27A	27B	28
Hf ppm	0·084		0·334	0·248		1·075	0·515	0·638	0·599
Lu ppm	0·126		0·003	0·2		0·008	0·133	0·166	0·003
$^{176}Lu/^{177}Hf$	0·213613		0·00113	0·113983		0·001091	0·036572	0·036724	0·000706
2 SE	0·001068		0·000006	0·00057		0·000005	0·000183	0·000184	0·000004
$^{176}Hf/^{177}Hf$	0·289631		0·28175	0·282494		0·282222	0·281781	0·281782	0·282012
2 SE	0·000038		0·000019	0·000023		0·000011	0·000021	0·000017	0·000021
Batch	13A	13B	14	15A	15B	16	17A	17B	18
Nd ppm	0·339212	0·328338	1·498575	0·559741	0·638444	3·764361	1·402225	1·453453	2·184537
Sm ppm	0·330559	0·316154	0·312158	0·390098	0·395003	0·747993	0·877249	0·872731	0·414042
$^{147}Sm/^{144}Nd$	0·589541	0·582498	0·12593	0·421324	0·374024	0·120114	0·378258	0·363046	0·114576
2 SE	0·00059	0·000582	0·000126	0·000421	0·000374	0·00012	0·000378	0·000363	0·000115
$^{143}Nd/^{144}Nd$	0·515433	0·515237	0·512468	0·512441	0·512357	0·512022	0·512957	0·512951	0·51222
2 SE	0·000095	0·00017	0·000015	0·000021	0·000017	0·000019	0·000015	0·000017	0·000047
$^{87}Sr/^{86}Sr$	0·700743			0·706284			0·705568		
2 SE	0·000025			0·000009			0·00002		
N	60			80			56		

(continued)

Table 3: Continued

	Roberts Victor			Bultfontein			
	DEJ02			B21		713	
	GT	CPX		GT	CPX	GT	CPX
Batch	29B	30		31	32	33	34
Hf ppm	0·258	0·483		0·732	1·893	0·163	2·509
Lu ppm	0·076	0·001		0·567	0·011	0·489	0·039
$^{176}Lu/^{177}Hf$	0·041921	0·000185		0·109497	0·000825	0·424337	0·002186
2 SE	0·00021	0·000001		0·000547	0·000004	0·002122	0·000011
$^{176}Hf/^{177}Hf$	0·282413	0·282236		0·282989	0·282656	0·290569	0·282775
2 SE	0·000024	0·000029		0·000018	0·000019	0·000017	0·000006
Batch	B	D	E	31	32	33	34
Nd ppm	3·321777	3·856425	1·354076	3·10524	21·763884	1·191256	44·054035
Sm ppm	0·586516	0·661175	0·815307	2·206177	3·895929	0·747749	6·583719
$^{147}Sm/^{144}Nd$	0·106738	0·103644	0·364024	0·429522	0·10822	0·379476	0·090341
2 SE	0·000107	0·000104	0·000364	0·00043	0·000108	0·000379	0·00009
$^{143}Nd/^{144}Nd$	0·512233	0·512255	0·512651	0·512537	0·512488	0·512478	0·51215
2 SE	0·000014	0·000029	0·000022	0·000008	0·000017	0·000007	0·000007
$^{87}Sr/^{86}Sr$	0·706108			0·705582		0·707226	
2 SE	0·000017			0·000023		0·000013	
N	40			95		195	

	Lovedale				Roodekraal	
	2073		2093		RDK1	
	GT	CPX	GT	CPX	GT	CPX
Batch	35	36	37	38	39	40
Hf ppm	0·204	1·391	0·109	1·954	0·090	1·535
Lu ppm	0·369	0·006	1·385	0·025	0·903	0·007
$^{176}Lu/^{177}Hf$	0·255514	0·00064	1·80355	0·001831	1·419229	0·000669
2 SE	0·001278	0·000003	0·009018	0·000009	0·007096	0·000003
$^{176}Hf/^{177}Hf$	0·28317	0·282402	0·286949	0·282901	0·303013	0·282289
2 SE	0·000011	0·000009	0·000019	0·000006	0·000018	0·000007
Batch	35	36	37	38	39	40
Nd ppm	2·301241	5·660012	2·210863	8·738373	0·372557	9·768035
Sm ppm	2·71026	1·547857	3·581014	2·914924	0·849691	2·989708
$^{147}Sm/^{144}Nd$	0·71205	0·165328	0·979309	0·201663	1·379962	0·185041
2 SE	0·000712	0·000165	0·000979	0·000202	0·00138	0·000185
$^{143}Nd/^{144}Nd$	0·512749	0·512478	0·512886	0·512433	0·516047	0·512595
2 SE	0·000006	0·000008	0·000008	0·000009	0·000006	0·000007
$^{87}Sr/^{86}Sr$	0·706887					
2 SE	0·000011					
N	95					

(continued)

Table 3: Continued

	Malaita	Roberts Victor			
	RG01	R30	DEJ03	DJ0288	DEJ02
Ma (Hf)	69	1953	129	−345	227
2 SE	12	13	12	37	47
initial $^{176}Hf/^{177}Hf$	0·282954	0·281708	0·282219	0·282017	0·282235
2 SE	0·00002	0·000019	0·000011	0·000021	0·000029
MSWD	4·14			0·02	
ε_{Hft}	8	5·9	−16·7	−34·2	−14
2 SE	0·5	0·6	0·4	0·4	0·7
Ma (Nd)	42	963	208	431	245
2 SE	6	42	18	91	25
initial $^{143}Nd/^{144}Nd$	0·512773	0·511672	0·511857	0·511906	0·512067
2 SE	0·00002	0·000045	0·00004	0·000216	0·000033
MSWD	0·2	2·4	2·2	10·6	2·8
ε_{Ndt}	3·5	5·2	−10·2	−3·6	−5·2
2 SE	0·3	0·5	0·4	2	0·4

	Bultfontein	Lovedale		Roodekraal	
	B21	713	2073	2093	RDK1
Ma (Hf)	164	981	161	120	778
2 SE	13	4	3	1	3
initial $^{176}Hf/^{177}Hf$	0·282653	0·282735	0·2824	0·282897	0·282279
2 SE	0·000019	0·000006	0·000009	0·000006	0·000007
MSWD					
ε_{Hft}	−0·6	20·4	−9·6	7	−0·3
2 SE	0·5	0·2	0·3	0·2	0·2
Ma (Nd)	23	173	76	89	441
2 SE	9	5	3	2	2
initial $^{143}Nd/^{144}Nd$	0·512471	0·512048	0·512396	0·512316	0·51206
2 SE	0·000022	0·000009	0·00001	0·000011	0·000008
MSWD					
ε_{Ndt}	−2·8	−7·3	−2·9	−4·2	−0·4
2 SE	0·2	0·1	0·1	1·8	0·1

and clinopyroxenes are in the range of $^{176}Hf/^{177}Hf = 0281750–0·282977$ and $^{143}Nd/^{144}Nd = 0·512022–0·512852$.

Jacob *et al.* (2005) showed how whole-rock analyses for such samples reflect metasomatic infiltration of the host kimberlite magma as well as chemical contributions from secondary components. Therefore, whole-rock data and epsilon values at the time of intrusion of the host magma (t) were calculated from mineral isotopic ratios and relevant elemental concentrations. Recalculated whole-rock data are in the range of $\varepsilon_{Nd} = -11·6 \pm 9·7$ and $\varepsilon_{Hf} = -32·8 \pm 31·3$.

In the eclogites and garnet pyroxenites Lu–Hf clinopyroxene–garnet mineral isochron ages are most often older than Sm–Nd clinopyroxene–garnet isochron minerals

ages by as much as 1000 Myr, and one eclogite from Roberts Victor (R30) has a clinopyroxene Rb–Sr model age of 3·15 Ga.

Roberts Victor

DEJ02. Three garnet and two clinopyroxene separates produced a Sm–Nd age of 245 ± 25 Ma with initial $^{143}Nd/^{144}Nd$ of 0·512067 ± 0·000033 and ε_{Ndt} of −5·2 ± 0·4. The Lu–Hf age for a different batch of separates was 227 ± 47 Ma, the initial $^{176}Hf/^{177}Hf$ 0·282235 ± 0·000029 and ε_{Hft} −14·0 ± 0·7. The $^{87}Sr/^{86}Sr$ ratio for the clinopyroxene is 0·706108 ± 0·000017.

DEJ03. Two garnet and one clinopyroxene separates produced a Sm–Nd age of 208 ± 18 Ma with an initial $^{143}Nd/^{144}Nd$ of 0·511857 ± 0·000040 and ε_{Ndt} of −10·2 ± 0·4. The Lu–Hf age calculated from analyses of a garnet and clinopyroxene pair (129 ± 12 Ma) is younger than that of the Sm–Nd system and the same as the age of entrainment by the host kimberlite (Fig. 2) with an initial $^{176}Hf/^{177}Hf$ of 0·282219 ± 0·000011 and a negative ε_{Hft} of −16·7 ± 0·4. The $^{87}Sr/^{86}Sr$ ratio for the clinopyroxene is 0·706284 ± 0·000009.

DJ0288. Two fractions of garnet (one leached and one unleached) and one fraction of clinopyroxene produced a Sm–Nd age of 431 ±91 Ma, with an initial $^{143}Nd/^{144}Nd$ of 0·511906 ± 0·000216 and ε_{Nd} of −3·6 ± 2. Lu–Hf analyses show that garnet is less radiogenic than the coexisting clinopyroxene. Garnets are invariant, with a $^{176}Hf/^{177}Hf$ initial ratio of 0·281781 ±0·000021, whereas clinopyroxenes yielded $^{176}Hf/^{177}Hf$ initial ratios of 0·282012 ± 0·000021, similar to other clinopyroxenes from the same locality. This anomalous isotopic disequilibrium has also been observed in similar samples by Jacob *et al.* (2005) and Simon *et al.* (2007).

R30. The Sm–Nd data for sample R30 are based on two fractions of garnet (15A, leached, and 15B) and one of clinopyroxene. Lu–Hf data were acquired from a different batch of garnet and clinopyroxene. This sample has a Sm–Nd age of 963 ± 42 Ma with initial $^{143}Nd/^{144}Nd$ of 0·511672 ± 0·000045 and ε_{Ndt} of 5·2 ± 0·5 and a Lu–Hf age of 1953 ± 13 Ma with initial $^{176}Hf/^{177}Hf$ of 0·281708 ± 0·000019 and ε_{Hft} of 5·9 ± 0·6 (Fig. 3). The clinopyroxene has a very unradiogenic $^{87}Sr/^{86}Sr$ ratio of 0·700743 ± 0·000025. This ratio gives a Rb–Sr model age of 3·15 Ga, calculated using the Bulk Earth values of Workman & Hart (2005).

Lovedale

02073. The Sm–Nd clinopyroxene–garnet mineral isochron produced an age of 76 ± 3 Ma, with an initial $^{143}Nd/^{144}Nd$ of 0·512396 ± 0·000010 and an ε_{Ndt} value of −2·9 ± 0·1. The Sm–Nd age coincides with the age of emplacement of the kimberlite host (74 Ma; Smith, 1983). The Lu–Hf clinopyroxene–garnet mineral isochron age from the same separates is 161 ± 3 Ma, with an initial $^{176}Hf/^{177}Hf$ of 0·282400 ± 0·000009 and an ε_{Hft} of −9·6 ± 0·3. The $^{87}Sr/^{86}Sr$ ratio for the clinopyroxene is 0·706887 ± 0·000011.

02093. The Sm–Nd clinopyroxene–garnet mineral isochron age is 89 ± 2 Ma with an initial $^{143}Nd/^{144}Nd$ = 0·512316 ± 0·000011 and an ε_{Ndt} of −4·2 ± 1·8. The Sm–Nd age is slightly older than the age of emplacement of the Lovedale pipes. The Lu–Hf clinopyroxene–garnet mineral isochron age for the same separates is 120 ± 1 Ma, with an initial $^{176}Hf/^{177}Hf$ of 0·282897 ± 0·000006 and an ε_{Hft} of 7·0 ± 0·2.

Roodekraal

RDK1. The Sm–Nd clinopyroxene–garnet mineral isochron age is 441 ± 2 Ma, with an initial $^{143}Nd/^{144}Nd$ of 0·512060 ± 0·000008 and a ε_{Ndt} of −0·4 ± 0·1. The Lu–Hf clinopyroxene–garnet mineral isochron age for the same garnet and clinopyroxene separates is 776 ± 3 Ma, with an initial $^{176}Hf/^{177}Hf$ = 0·282279 ± 0·000007 and ε_{Hft} of −0·3 ± 0·2.

Bultfontein

B21. The Sm–Nd clinopyroxene–garnet isochron age is 23 ± 9 Ma, with an initial $^{143}Nd/^{144}Nd$ of 0·512471 ± 0·000022 and an ε_{Ndt} of −2·8 ± 0·2. Lu–Hf analyses for the same separates provide a clinopyroxene–garnet mineral isochron age of 164 ± 13 Ma, with an initial $^{176}Hf/^{177}Hf$ of 0·282653 ± 0·000019 and an ε_{Hft} of −0·6 ± 0·5. Whereas the Sm–Nd is reset to an age younger than the emplacement age, the Lu–Hf age is still older than the known age of kimberlite emplacement (84 ± 1 Ma, Rb–Sr on phlogopite, Kramers *et al.* 1983). The $^{87}Sr/^{86}Sr$ for the clinopyroxene is 0·705582 ± 0·000023.

713. The Sm–Nd clinopyroxene–garnet mineral isochron gives an age of 173 ± 5 Ma, with an initial $^{143}Nd/^{144}Nd$ of 0·512048 ± 0·000009 and an ε_{Ndt} of −7·3 ± 0·1. The Lu–Hf clinopyroxene–garnet mineral isochron age is 981 ±4 Ma, with an initial $^{176}Hf/^{177}Hf$ of 0·282735 ± 0·000006 and a positive ε_{Hft} of 20·4 ± 0·2. The $^{87}Sr/^{86}Sr$ for the clinopyroxene is 0·707226 ± 0·000013.

Malaita

RG01. Two fractions of clinopyroxene (I and J) and two fractions of garnet (G and H2) from sample RG01 were analysed for Sm and Nd isotopes; fraction G was leached. The Sm–Nd data yield an age of 42 ± 6 Ma with an initial $^{143}Nd/^{144}Nd$ of 0·512773 ± 0·000020 and ε_{Ndt} of 3·5 ± 0·3. Lu–Hf analyses for all mineral fractions plus three previous garnet fractions (A, B and H1) yield an age of 69 ± 12 Ma with an initial $^{176}Hf/^{177}Hf$ of 0·282954 ± 0·000020 and an ε_{Hft} of 8·0 ± 0·5. The $^{87}Sr/^{86}Sr$ ratio from the clinopyroxene is 0·703812 ± 0·000013.

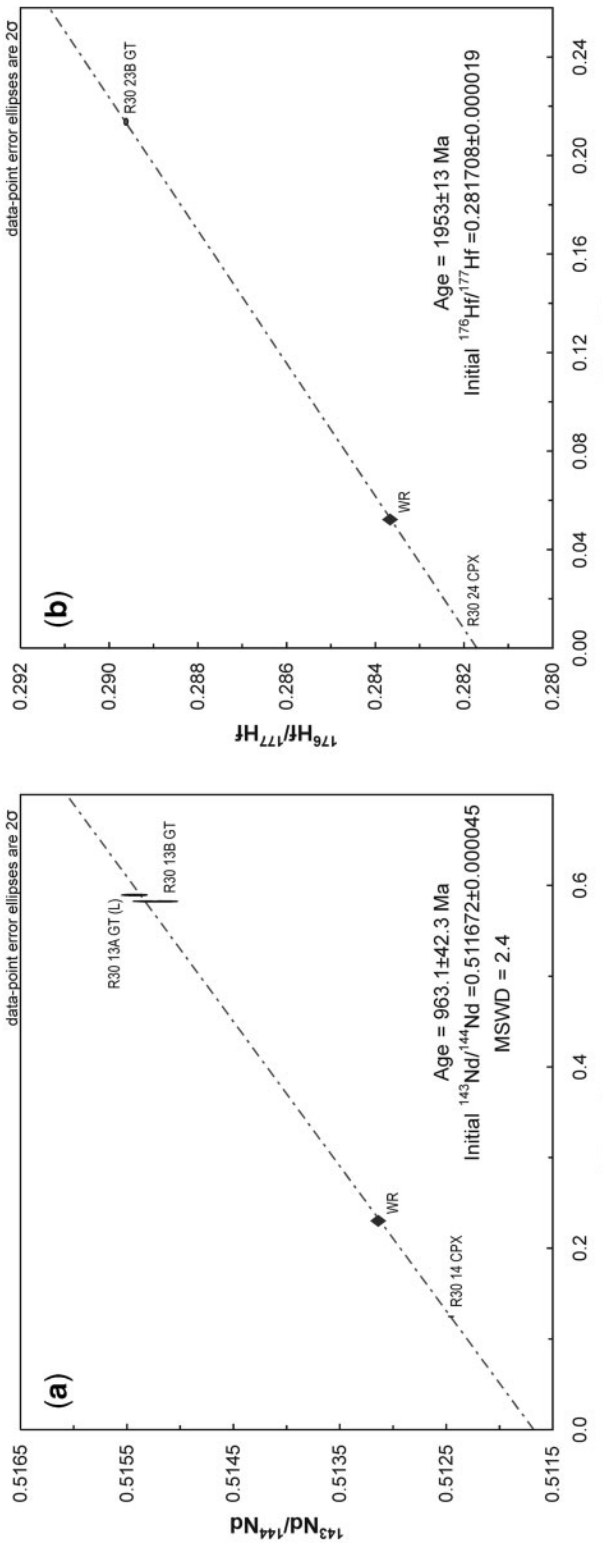

Fig. 3. (a) Sm–Nd and (b) Lu–Hf clinopyroxene–garnet mineral isochrons giving Proterozoic ages for Roberts Victor eclogite R30 entrained in a kimberlite at 127 Ma. This is in marked contrast to the Archaean Rb–Sr model age based on clinopyroxene and reconstructed whole-rock data (see text).

Table 4: Lu–Hf and Sm–Nd data for garnet pyroxenites and eclogites (all ages in Ma)

Rock type and location	Sample	Lu–Hf cpx–gt age	Sm–Nd cpx–gt age	Emplacement or entrainment age
Garnet pyroxenites				
Malaita (this study)	RG01	69 ± 11·7	41·6 ± 5·6	34–35
Bultfontein (this study)	713	980·0 ± 4·4	173·4 ± 5·1	84
	B21	164·1 ± 12·6	23·3 ± 8·8	
Norway (Lapen *et al.*, 2005)	41-1	1266 ± 6	1155 ± 8	
	41-2	1190 ± 6·2	1125 ± 7·7	
Beni Bousera (Pearson & Nowell, 2004)	GP37	16·8 ± 6·6	40·5 ± 2·3	22
	GP139	22·5 ± 1·1	19·9 ± 1·7	
	GP147	20·8 ± 2·5	19·1 ± 1·1	
Beni Bousera (Blichert-Toft *et al.*, 1999)	M5-10	25·3 ± 1·2	24·0 ± 4·3	
Bearpaws USA (Scherer *et al.*, 2000)	RRE5a	1502 ± 13; 1522 ± 12	1363 ± 13	
Eclogites				
Lovedale, SA (this study)	0207335	161·3 ± 3	75·8 ± 2·7	70–130
	0209337	120·3 ± 0·7	89·0 ± 2·3	
Rodekraal, SA (this study)	RDK1	777·7 ± 3·1	441 ± 1·5	
Roberts Victor (this study)	R30	1953 ± 13	963·1 ± 42·3	127
	DEJ02	226·9 ± 47·2	245 ± 24·7	
	DEJ03	129 ± 12	207·8 ± 18·5	
Roberts Victor (Jacob *et al.*, 2002)	BD1191	1400	907	
	BD1175	494	221	
	BD3699	394	110	
	RV1	199	−0·9	
	DE55	2·230	1·194	
	HRV247	23	146	
Himalayas (de Sigoyer *et al.*, 2000)	Ts34	55 ± 12		65–45
	Ch157a		55 ± 7	
	Ts45		47 ± 11	
California (Anczkiewicz *et al.*, 2004)	PG5	114·5 ± 0·6	130 ± 43	160–140
	PG31	157·9 ± 0·7	178 ± 11	
China (Cheng *et al.*, 2008)	04HZ44a	224 ± 1·9	217·8 ± 6·1	240–205
	04HZ15b	240 ± 5·0	222·5 ± 5	
	04SM20a	230 ± 5	224·2 ± 2·1	

Data for garnet pyroxenites from Blichert-Toft *et al*. (1999), Scherer *et al*. (2000) and Pearson & Nowell (2004), and for eclogites from de Sigoyer *et al*. (2000), Jacob *et al*. (2002), Anczkiewicz *et al*. (2004) and Cheng *et al*. (2008).

DISCUSSION

Lu–Hf and Sm–Nd ages in eclogites and garnet pyroxenites

Published data suggest that the Lu–Hf system gives more robust ages than the Sm–Nd system (e.g. Blichert-Toft *et al.*, 1999; Scherer *et al.*, 2000; Bedini *et al.*, 2002). It has been argued that, compared with the Sm–Nd system, the Lu–Hf system remains relatively undisturbed during thermo-tectonic processes (Jacob *et al.*, 2002; Stevenson *et al.*, 2002). In this study, in which Sm–Nd and Lu–Hf data were determined on the same clinopyroxene–garnet pairs from eclogites and garnet pyroxenites, we agree with the above conclusion in the majority of instances; however, other issues have arisen that affect the straightforward interpretation of Lu–Hf data.

The Sm–Nd and Lu–Hf age information is summarized in Table 4 and compared with published data for eclogites

and garnet pyroxenites (i.e. orogenic massifs and xenoliths). The Lovedale eclogites have a range of Sm–Nd and Lu–Hf ages that straddle the age of entrainment (70–130 Ma) and, as such, were probably reset by entrainment in the host kimberlite. In contrast, the Roodekraal eclogite gave Sm–Nd and Lu–Hf clinopyroxene–garnet isochron ages that differ from the age of entrainment; the Lu–Hf age is older than the Sm–Nd age by *c.* 336 Myr. One Kimberley eclogite gave identical Sm–Nd and Lu–Hf clinopyroxene–garnet isochron ages, 100 Myr older than the age of entrainment (127 Ma). For another Kimberley eclogite an unusual situation arises. The Sm–Nd clinopyroxene–garnet isochron age is older then the Lu–Hf clinopyroxene–garnet isochron age by 79 Myr and the Lu–Hf age is the same as the age of entrainment (127 Ma). A Roberts Victor eclogite (R30) has Sm–Nd and Lu–Hf clinopyroxene–garnet isochron ages that differ markedly from the age of entrainment (127 Ma). The Sm–Nd age is *c.* 835 Myr older than the age of entrainment; more importantly, the Lu–Hf clinopyroxene–garnet isochron age is 990 Myr older than the Sm–Nd clinopyroxene–garnet isochron age. For the same eclogite the Rb–Sr clinopyroxene model age is 3·15 Ga based on the lowest $^{87}Sr/^{86}Sr$ ratio measured to date in a clinopyroxene. This raises the issue of the extent to which the apparently more robust Lu–Hf system actually records the original protolith age.

Although Lu–Hf and Sm–Nd analyses were performed on different eclogite samples and hence different clinopyroxene–garnet separates (de Sigoyer *et al.*, 2000), the orogenic eclogites from the western Himalayas have identical Lu–Hf and Sm–Nd mineral ages (55 Ma). This age overlaps with the age of emplacement of the orogenic system. This pattern is confirmed by studies of other orogenic garnet pyroxenites from Beni Bousera, Morocco (Blichert-Toft *et al.*, 1999; Pearson & Nowell, 2004). These data reveal overlapping Sm–Nd and Lu–Hf ages for the bulk of the samples analysed (with the exception of one sample) (Table 4). Although the data of Blichert-Toft *et al.* (1999) appear slightly older (Table 4), the data are within error of the more extensive study of Pearson & Nowell (2004) and the majority of the data are within error of the age of emplacement of the massif. More significant differences in age between Lu–Hf and Sm–Nd mineral isochrons (Table 4) were reported for Proterozoic garnet pyroxenites (*c.* 1120 Myr) from the Sandvik orogenic garnet peridotite massifs (Lapen *et al.*, 2005). Lu–Hf mineral isochrons record events that are *c.* 60–100 Myr older than the Sm–Nd ages. This is evident in some of the data reported herein. A possible explanation for the differences between the Lu–Hf and Sm–Nd ages is provided by a recent study of chemically zoned garnets in eclogites from the Dabie Orogen, China (Cheng *et al.*, 2008). This work reveals that older Lu–Hf mineral isochron ages (224–240 Ma) may record high-temperature garnet growth at 'peak' metamorphic conditions compared with younger Sm–Nd ages (217–224 Ma) that may relate to 'retrograde' overgrowths produced at lower temperatures. Eclogites from the Franciscan Coastal Ranges of California (Anczkiewicz *et al.*, 2004) are more complicated: (1) Lu–Hf ages are different for different eclogites from the same locality; (2) one eclogite has a Sm–Nd clinopyroxene–garnet isochron age that records an older age than the Lu–Hf clinopyroxene–garnet mineral isochron; (3) Lu–Hf data are either similar to, or younger than emplacement ages; (4) Sm–Nd ages are 'older' than Lu–Hf ages and overlap with, or are close to, the age of emplacement. Clearly, further work is required to clarify these complex relationships in orogenic eclogites and garnet pyroxenites.

Gonzaga (2007) attempted to evaluate temperatures and pressures of equilibration for the rocks analysed in this study. Because of their restricted parageneses and the need for different diffusion coefficients for different pyroxene compositions, calculations were restricted to cation exchange and oxygen isotope thermobarometers or thermometers. A number of errors can be introduced in these calculations, notably a dependence on the determination of the oxidation state of Fe for cation exchange based thermometers. Additionally, oxygen isotope based thermometers have been shown to be less reliable, with large ranges in calculated temperatures resulting from analytical error. Nevertheless, the results compare favourably with published values for similar lithologies from the same localities. Temperatures and pressures calculated for oceanic settings indicate equilibration within the spinel and garnet peridotite stability fields (1000–1100°C at pressures of 9–15 kbar), followed by resetting of the oxygen isotope based temperatures by the host basalt or alnöite during emplacement. Samples from cratonic settings display a more complex history, reflecting polybaric metamorphism of a subducted slab up to ultrahigh-pressure conditions. This complexity is recorded in the formation of alteration rims and resetting of oxygen isotope based temperatures by the host kimberlite during emplacement.

Because basalt- and kimberlite-hosted eclogites and garnet pyroxenites appear to have experienced much higher temperatures (*c.* 1300°C) than orogenic eclogites or garnet pyroxenites, the behaviour of the isotope systems is different. In addition, some of these samples have undergone retrograde reactions (i.e. eclogite to garnet pyroxenite), evident by a change in pyroxene composition from omphacite to augite (Table 1; Gonzaga, 2007). High-temperature alnöite-hosted garnet (±quartz) pyroxenites from Malaita have similar Lu–Hf and Sm–Nd ages that overlap (within error) with the age of entrainment in the alnöite (i.e. 34 Ma; Ishikawa *et al.* 2007). However, a garnet pyroxenite from Malaita (with smaller analytical errors), shows different behaviour (Table 4). The Lu–Hf

clinopyroxene–garnet isochron age (69 ± 11·7 Ma) is older than the Sm–Nd clinopyroxene–garnet isochron age (41·6 ± 5·6 Ma) (Table 4) by *c.* 10 Myr. Whereas the Sm–Nd age is within error of the entrainment age, the Lu–Hf age is similar to that of older tholeiitic magmatic episodes evident on San Cristobal in the Solomon Islands (~62 Ma ^{40}Ar–^{39}Ar age). These are compositionally similar to plume-related basalt magmatism at ~90 Ma (Birkhold-VanDyke *et al.*, 1996; Tejada *et al.*, 2002). This may indicate that at magmatic temperatures (and during diatreme formation) Lu–Hf is more robust than Sm–Nd and retains the original protolith age (Table 4; Gonzaga, 2007). This is supported by Lu–Hf and Sm–Nd data for an eclogite from the Bearpaws Mountains (Scherer *et al.*, 2000). This eclogite has a Lu–Hf clinopyroxene–garnet isochron age (1502–1522 Ma) that is older than the Sm–Nd clinopyroxene–garnet isochron age (1363 Ma) by *c.* 240 Myr. Kimberlite-hosted garnet pyroxenites from Bultfontein (Table 4) support the contention that Lu–Hf is more robust, with an age difference of 707 Myr between the Sm–Nd and Lu–Hf mineral isochrons.

In cratonic eclogites (>2·5 Ga) a clear potential exists for Archaean protolith ages to be obtained. However, these may be lost as a result of their residence time within the craton and subsequent entrainment in high-temperature, volatile-rich kimberlite magmas. The Sm–Nd mineral isochron ages for the Lovedale eclogites (75·8–89 Ma) have been reset by entrainment (70–130 Ma) and it could also be surmised that the Lu–Hf mineral isochrons record partial resetting (120–161 Ma). The Roodekraal eclogite Lu–Hf and Sm–Nd mineral ages differ from the age of entrainment by 300–640 Myr and again the Lu–Hf system appears to be more robust than Sm–Nd. Two Kimberley eclogites have identical (within error) Lu–Hf and Sm–Nd mineral isochron ages and one sample has a Lu–Hf age identical to the age of entrainment (127 Ma) and an older Sm–Nd mineral isochron age.

The Roberts Victor eclogites have been the focus of several studies. In a pioneering piece of work Jagoutz *et al.* (1984) determined a Sm–Nd age of 2700 ± 100 Ma for the eclogites. Jacob *et al.* (2005) extended the dataset and obtained a similar Sm–Nd age of 2763 ± 330 Ma and a Lu–Hf age of 2349 ± 140 Ma, noting a wide range of Sm–Nd and Lu–Hf clinopyroxene–garnet mineral ages. Although there is a lack of consistency in the ages, the majority of the eclogites demonstrated that the Lu–Hf system tends to record older events. In some instances the Lu–Hf and Sm–Nd ages differ by *c.* 500 Myr, whereas in others meaningless future ages were obtained. Because of this issue Jacob *et al.* (2005) adopted a different strategy, involving reconstructed whole-rocks. The Lu–Hf reconstructed whole-rock age was within error of the original Sm–Nd whole-rock isochron age (Jagoutz *et al.*, 1984) and the isochron age from Jacob *et al.* (2005).

In this study five out of six eclogites from the Kaapvaal craton gave older Lu–Hf ages than the Sm–Nd system, with differences in clinopyroxene–garnet mineral ages ranging from 31–900 Myr (Table 4). One Roberts Victor eclogite yielded a Lu–Hf clinopyroxene–garnet age (1953 Ma) that is *c.* 1000 Myr older than the Sm–Nd clinopyroxene–garnet age of 963 Ma. However, it should be noted that neither of these ages compare favourably with the Roberts Victor reconstructed whole-rock ages, despite the fact that sample R30 is included in the revised whole-rock age calculation (Fig. 4). In fact, it seems that the dataset from Jagoutz *et al.* (1984) is strongly controlled by two samples with extremely radiogenic isotopic compositions, which were not observed in the data of Jacob *et al.* (2005) or this study. This strongly suggests that the Roberts Victor eclogites are not all cogenetic and/or comagmatic. However, this may not matter because the true age of the eclogites may differ from the age determinations based on Lu–Hf and Sm–Nd mineral isochrons and recalculated whole-rocks. This is best illustrated by a clinopyroxene from eclogite R30: although some examples in the literature show very low $^{87}Sr/^{86}Sr$ (e.g. Pearson *et al.*, 1995; Jacob *et al.*, 2005), sample R30 has the lowest $^{87}Sr/^{86}Sr$ of any clinopyroxene analysed to date ($^{87}Sr/^{86}Sr = 0{\cdot}700743 \pm 0{\cdot}000025$) (Gonzaga, 2007). The resulting Rb–Sr model age of 3·15 Ga is within error of the Sm–Nd whole-rock age (Jacob *et al.*, 2005). In addition, it compares favourably with U–Pb ages of zircons (Shirey *et al.*, 2004) that suggest an age of 3061 ± 6 Ma for the Roberts Victor eclogites.

Eclogites and garnet pyroxenites

Cratonic eclogites (Kaapvaal) from this study have heterogeneous Hf–Nd–Sr isotope ratios that define a positive trend on a Hf–Nd isotope diagram (Fig. 5) similar to mantle-derived ocean island basalt (OIB) and kimberlitic magmas but also similar to complex upper mantle peridotites entrained from beneath cratons. In addition, the negative array on a Nd–Sr isotope diagram (Fig. 6) attests to a possible petrogenetic link with oceanic magmatism and megacrysts in kimberlites. The isotopic similarities to such magma compositions may be a primary feature related to protolith formation or an artefact of secondary processes involving pre- or syn-entrainment interaction with the host magmas. Despite the fact that the Hf–Nd–Sr isotope variability in the eclogites encompasses the complete range of depleted to enriched 'oceanic' mantle compositions (e.g. OIB, kimberlites), many eclogites plot outside the field of oceanic basalts and have more 'crustal' isotopic signatures. Published data for the Roberts Victor eclogites show that they encompass the entire range of Hf–Sr–Nd variability for most mantle and some crustally derived rocks (e.g. Jacob *et al.*, 2005).

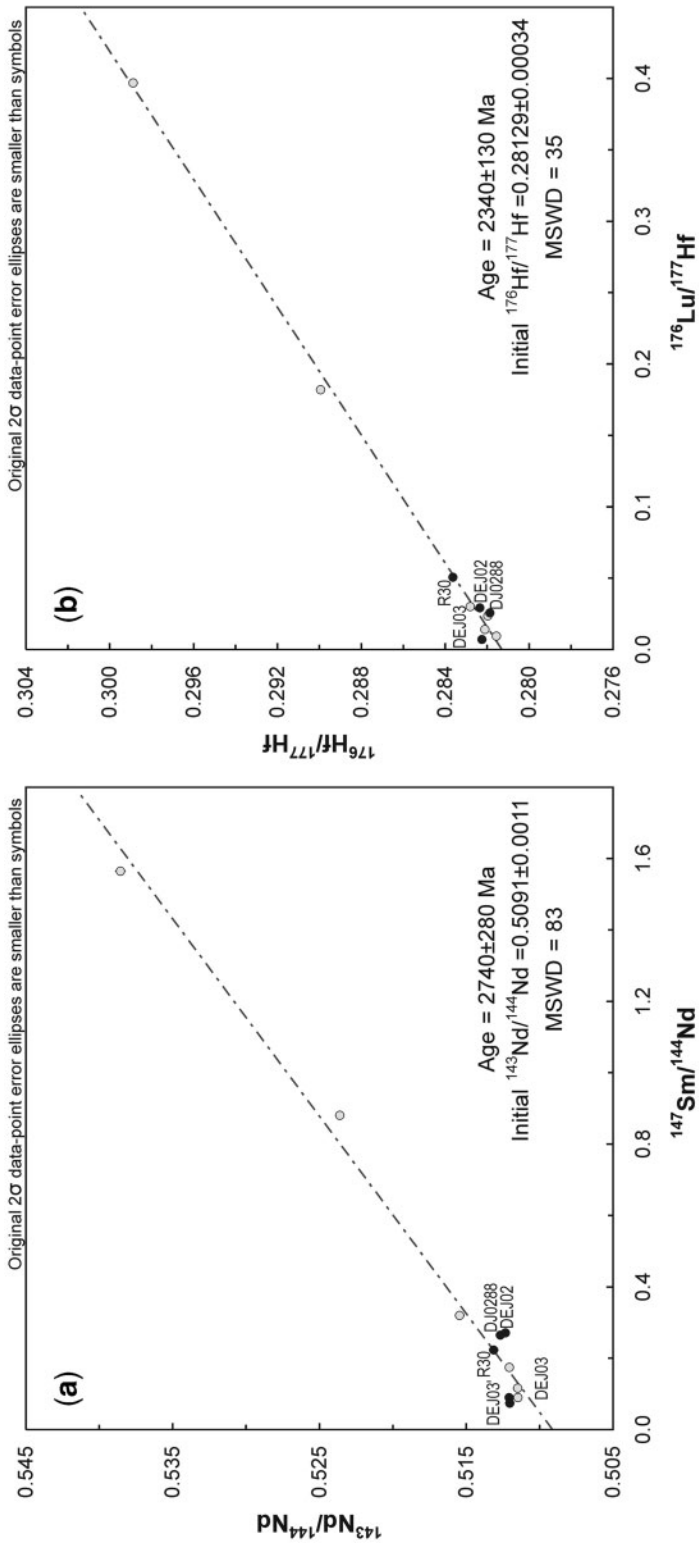

Fig. 4. (a) Sm–Nd and (b) Lu–Hf isochron based on recalculated whole-rock data for Roberts Victor eclogites (Jagoutz *et al.*, 1984; Jacob *et al.*, 2005; this study). Error ellipses assumed at 5% are too small to be plotted and hence were replaced by symbols. It should be noted that the gradient is strongly controlled by two highly radiogenic samples. (Compare this isochron age with Proterozoic age data for Roberts Victor eclogite R30 in Fig. 3 and the Archaean age obtained for the clinopyroxene.)

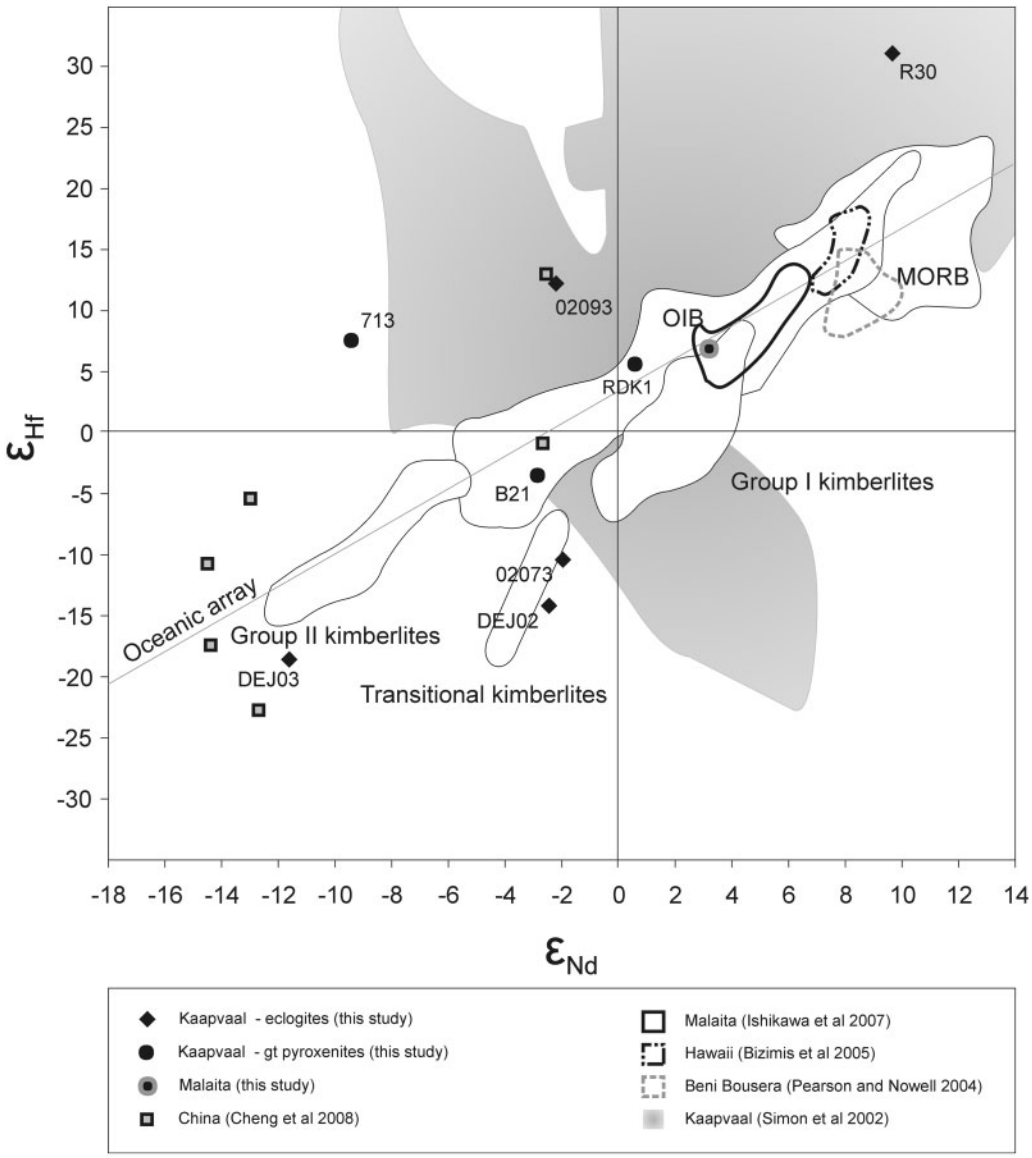

Fig. 5. Hf–Nd isotope variation for eclogite and garnet pyroxenite calculated bulk compositions (adapted from Nowell *et al.*, 2004). It should be noted that the analysed samples define a positive Hf–Nd isotope correlation. The data overlap with the Kaapvaal mantle xenoliths (shaded field, Simon *et al.*, 2002) or OIB–Group II–transitional kimberlites reinforces a genetic link with shallow mantle processes and metasomatism by host kimberlite magmas. The Malaita garnet pyroxenite in this study lies within the range of Hf–Nd isotope compositions reported by Ishikawa *et al.* (2007).

Specifically the eclogites have Hf–Nd–Sr isotopic affinities with:

(1) garnet peridotites from the Kaapvaal craton that have had a complex history spanning over 3 Gyr, during which time they have variably interacted with magmas traversing the cratonic keel (e.g. Nowell *et al.*, 2004, and references therein);
(2) Group II and transitional kimberlites, which are in part responsible for the heterogeneity observed in (1) because of interaction with the mantle lithosphere during magma transfer (e.g. Becker & LeRoex, 2006, and references therein);
(3) Group II kimberlite megacrysts, mainly garnet and clinopyroxene, which could be derived from eclogite or garnet pyroxenite precursors, disrupted during crack propagation and magma transfer involving the magmas in (2).

The isotopic heterogeneity displayed by the Kaapvaal cratonic eclogites cannot be reconciled with a common source. Gonzaga (2007) attempted to model the evolution

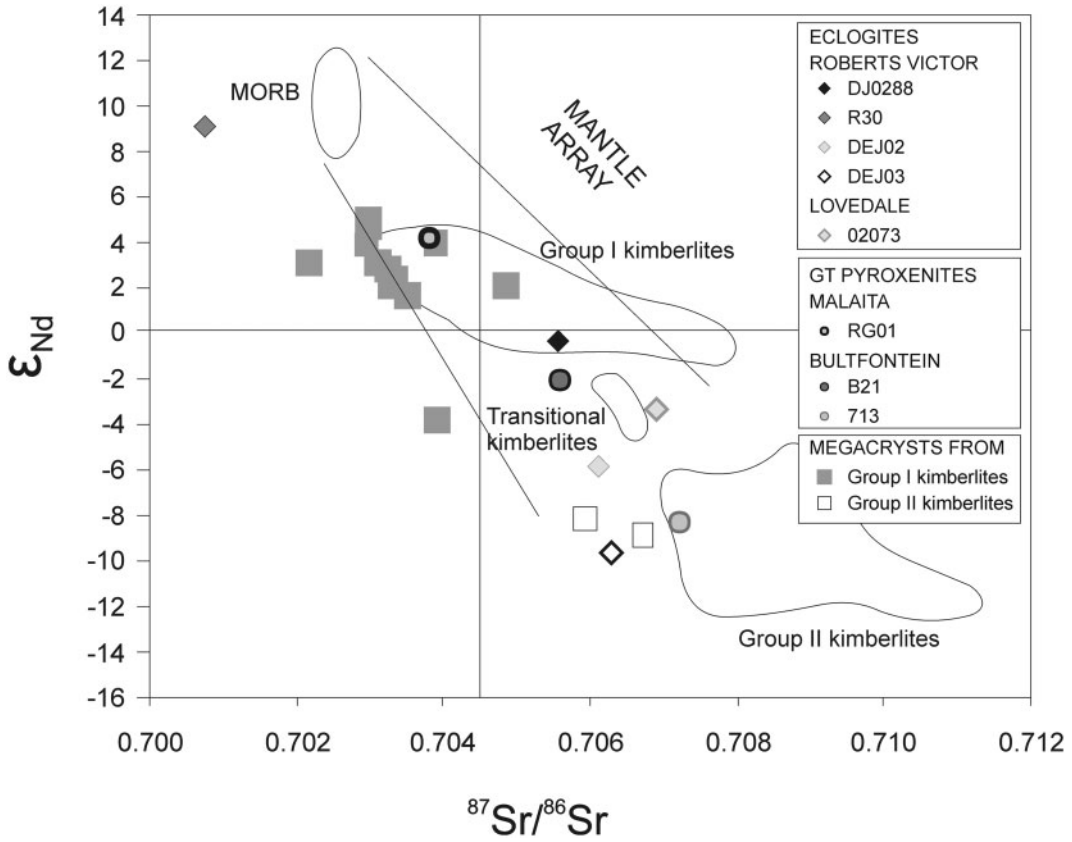

Fig. 6. Nd–Sr isotope variation at the time of emplacement for cratonic garnet pyroxenites and cratonic eclogites (adapted from Nowell *et al.*, 2004). The Roberts Victor eclogites display a general anti-correlation from ultra-depleted to enriched compositions and overlap with Group II megacrysts (garnet and pyroxene) and kimberlites. Less depleted than MORB, the garnet pyroxenites plot toward more enriched compositions in the field of ocean-island basalts and kimberlites, as is the case for Hf–Nd isotopes. The similarity should be noted between eclogite and garnet pyroxenite data and Group II megacrysts (clinopyroxene and garnet), raising the possibility that the megacrysts are disrupted eclogites or garnet pyroxenites. Group I megacrysts are similar to the Malaita garnet clinopyroxenite—interpreted to be a high-temperature derivative of a mantle-derived tholeiitic melt.

of such rocks from an Archaean oceanic mantle source (*c.* 3 Ga; Shirey *et al.*, 2004) through possible events including subduction (*c.* 2·7 Ga; Poujol *et al.*, 2003), partial melting and metasomatism by passing kimberlite-like melts and/or by the host kimberlite at around 128 Ma. Epsilon values calculated at the present day, 128 Ma, 2700 Ma and 3450 Ma show different trajectories, even when isotopic ratios calculated at the present day are similar (Fig. 7). The distinct trajectories despite similarities in isotopic ratios are a consequence of different concentrations of Sm, Nd, Lu and Hf and as such cannot be ascribed to specific events at 128 Ma, 2700 Ma or 3450 Ma. Therefore, the inverse modelling of the source of these samples is not feasible.

Forward modelling (Fig. 8) was based on the compositions of komatiites and basalts from 2·7 and 3·45 Ga greenstone belts in Southern Africa (Blichert-Toft & Arndt, 1999) which are both similar to and older than the supposed age of the subduction event and spatially associated with the eclogite xenoliths. The evolutionary trend of the komatiites from the 2·7 Ga greenstone belts follows that of the 3·45 Ga belts. Samples from the Barberton greenstone belt are similar to estimates for mid-ocean ridge basalt (MORB) mantle at around 3·0 Ga (e.g. Nowell *et al.*, 2004). However, calculated present-day values for the selected Archaean source result in a much distinct and more delimited range of negative ε_{Hf} and ε_{Nd} values than the samples studied. This excludes possibility of an origin directly from a basaltic melt.

Trace element and oxygen isotope data (Gonzaga *et al.*, 2009) suggest subduction and possibly partial melting of an oceanic crust protolith as part of the process of formation of eclogites. Consequently, the suggestion that some of the samples included in this dataset may represent residues after *c.* 6% point average fractional melting of a source similar to the Barberton komatiites in equilibrium with tonalitic melts (Gonzaga, 2007) was also evaluated (Fig. 8). The evolution of such a garnet-bearing residue

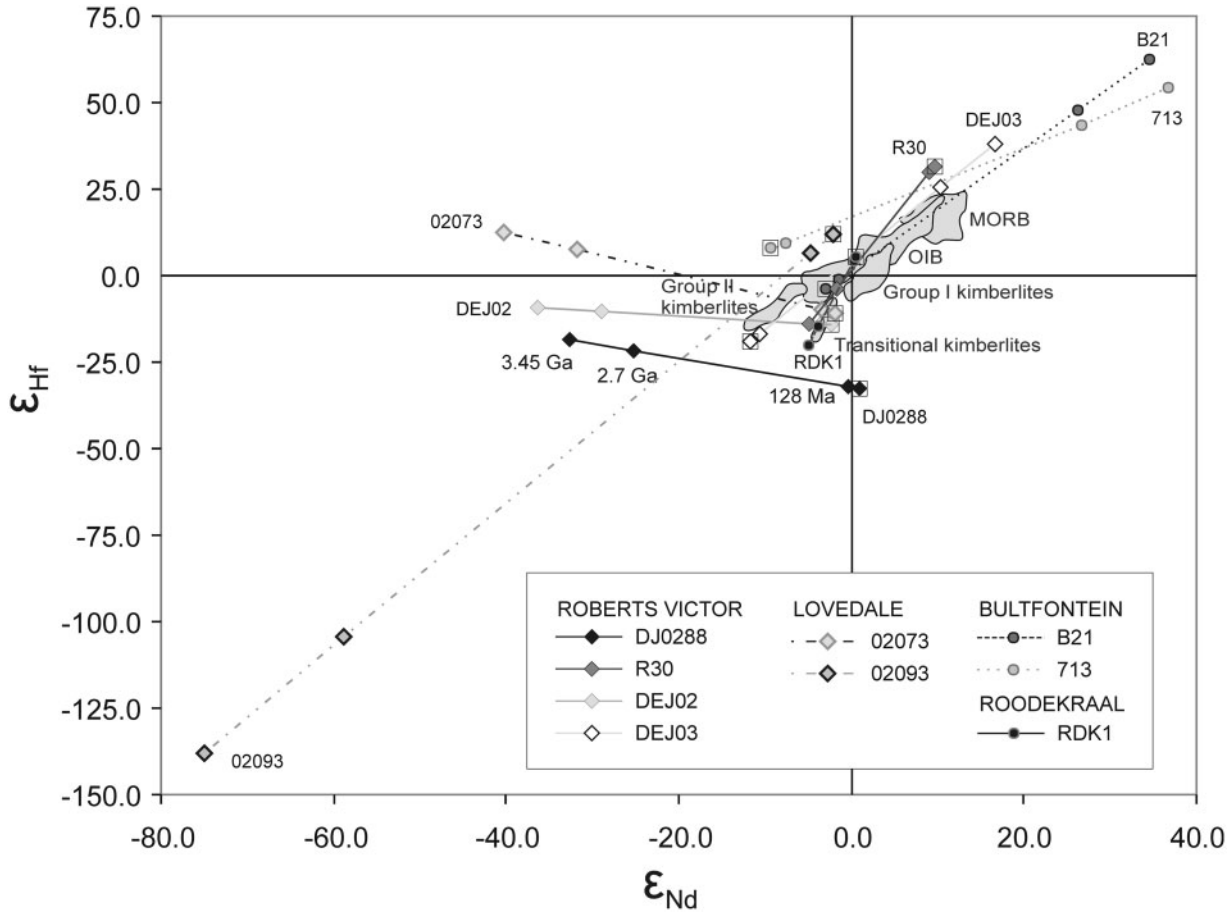

Fig. 7. Plot of ε_{Nd} vs ε_{Hf} for eclogites and garnet pyroxenites at present (open square around sample symbols), 128 Ma, 2·7 Ga and 3·45 Ga. OIB, MORB and kimberlite fields from Pearson & Nowell (2004) are presented for reference.

follows a trajectory towards more positive ε_{Hf} and ε_{Nd} values, reaching values similar to those for Group I kimberlites at 128 Ma. Further mixing with either Group I or II kimberlites host would result in a range of mostly negative ε_{Hf} values. Therefore, a partial melt event (with possible mixing with the kimberlite host) cannot account for all the isotopic variation observed in this dataset.

Bedini *et al.* (2004) evaluated a model for the diffusion of radiogenic Sm, Nd, Lu and Hf isotopes in low-temperature garnet peridotite xenoliths from South African kimberlites. They showed that as metasomatism by kimberlite affected radiogenic/unradiogenic ratios, garnet and clinopyroxenes were neither isotopically nor chemically equilibrated. Furthermore, later crystallization of pyroxene could result in negative Sm–Nd ages, similar to those observed in this study as well as those reported by Jacob *et al.* (2005) and Simon *et al.* (2007). Bedini *et al.* (2004) suggested that diffusion of radiogenic Hf in garnet is slower than in pyroxene and as a result evidence of their cooling history may still be preserved in the core of garnets. However, for the samples analysed in this study (1) there is no evidence of zonation in the garnets (Gonzaga, 2007) and (2) careful petrographic study of the samples, combined with leaching, has demonstrated the absence of additional phases that could be a repository for radiogenic Hf, such as phosphate (see 'Analytical techniques').

Oxygen isotope, trace element and mineral chemistry data in this study (Gonzaga 2007) also indicate the possible metasomatic effects of kimberlite-like melts on most of the samples. Mixing with the host kimberlite (Group I and Group II kimberlites) during entrainment is not sufficient to account for all the variability showed in the dataset (Gonzaga, 2007). However, there is no method to establish accurately the timing, the source and the extent of metasomatism, as it can be a result of multiple events at various times. For example, Simon *et al.* (2007) listed seven large-scale events that may have resulted in metasomatism of the mantle in the Kaapvaal region from crust formation in the Archaean to kimberlite magmatism at 90 Ma.

Nowell *et al.* (2004) calculated the effects of metasomatism by addition of 0·1–10% Group I kimberlite or picritic melt to 3 Ga Depleted Continental Mantle at various

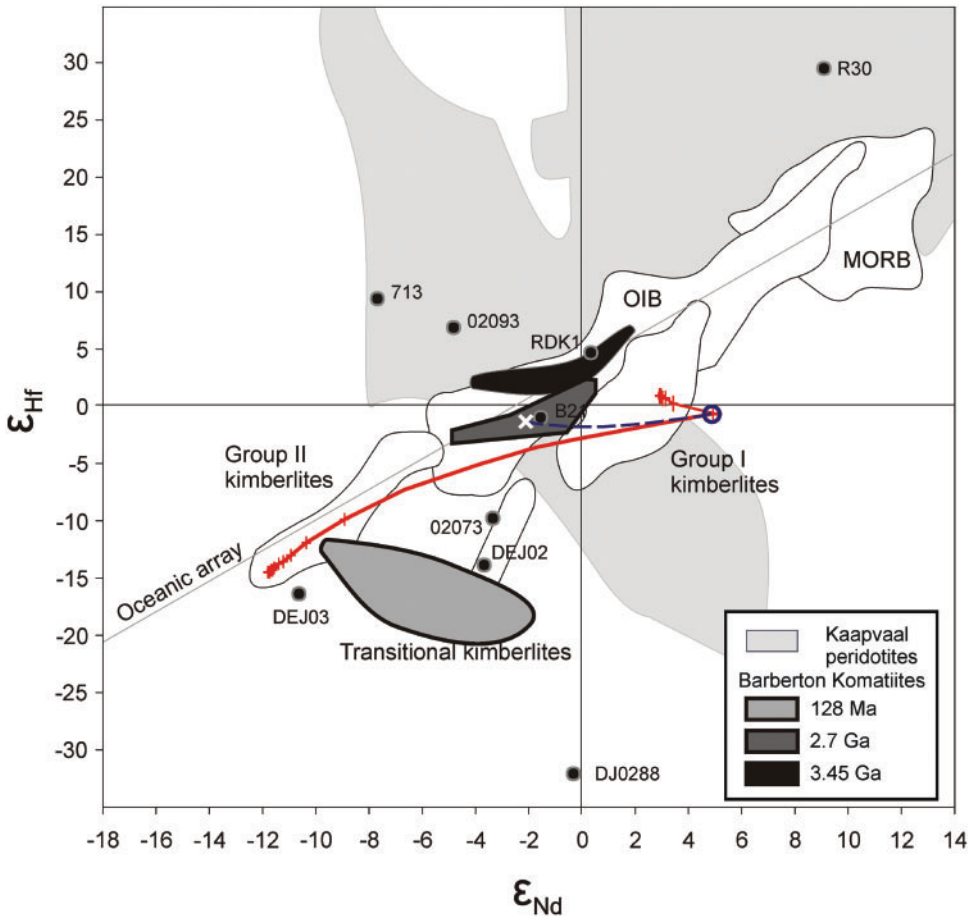

Fig. 8. Variation of ε_{Nd} vs ε_{Hf} at 128 Ma for eclogites and garnet pyroxenites from the Kaapvaal craton (adapted from Pearson & Nowell, 2004). Shaded area represents data for Kaapvaal peridotites from Simon *et al.* (2002). Also shown are fields for komatiites from the Barberton Greenstone Belt (Blichert-Toft & Arndt, 1999) at 3·45 Ga, 2·7 Ga and 128 Ma representing, respectively, formation of the protolith, subduction and emplacement of the kimberlite host. The white cross represents the Hf–Nd isotope composition of a 6% point average fractional partial melt at the time of subduction (2·7 Ga) as suggested by trace element and oxygen data (Gonzaga *et al.*, 2009). Blue dashed curve represents the evolution of the residue of this melting event until the time of emplacement of Group II kimberlites (128 Ma, blue open circle). This value is practically indistinguishable from values recalculated to the time of emplacement of Group I kimberlites. Red continuous curves represent mixing curves from this residue and Group II kimberlites at 128 Ma and from this residue and Group I kimberlites at 74 Ma (crosses indicating 10% mixing intervals).

times from 1·5 Ga. The resulting field ranges towards very positive ε_{Hf} and ε_{Nd} values and encompasses the majority of the samples from this study, unlike any of the previous approaches for either inverse or forward modelling (Fig. 9). Additionally, metasomatic exchange may be responsible for the unfeasible ages for samples B21 and DJ0288 as observed for other samples from the Kaapvaal craton by Simon *et al.* (2007).

Cratonic (Bultfontein) and oceanic (Malaita) garnet pyroxenites are less isotopically heterogeneous than continental eclogites, not only for Sr–Nd–Hf but also for O isotopes. In general garnet pyroxenites plot on, or in the vicinity of, the 'oceanic mantle array' and show similarities to OIB and Group I and II kimberlites. Like eclogites, garnet pyroxenites from Kaapvaal (Fig. 6) have Sr–Nd isotope variations similar to those of transitional kimberlites and Group II megacrysts (garnet and clinopyroxene). Nowell *et al.* (2004) studied Group II megacrysts and linked them to Group II kimberlites. They argued that ancient, deeply subducted oceanic basalt (eclogite) must have been part of the reservoir from which kimberlites were formed and that this reservoir was subsequently disrupted and entrained. Similarly, Becker & LeRoex (2006) proposed that the source of Group I and II kimberlites is within the subcontinental lithospheric mantle (Archaean–Proterozoic in age) that has been previously metasomatized. In the case of Group I kimberlites metasomatism involved plume-derived melts or, in the case of Group II kimberlites, subduction-related melts. This distinction is consistent with O isotope data from the xenoliths

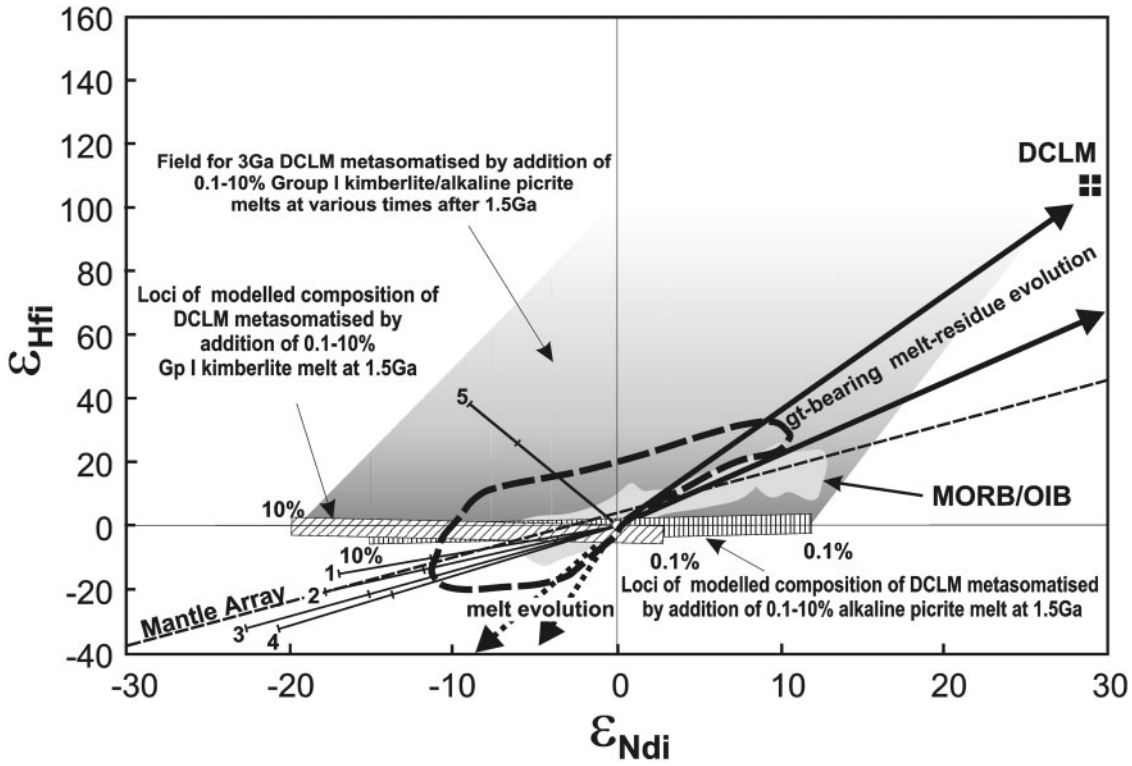

Fig. 9. Effects of kimberlitic metasomatism on 3 Ga Depleted Continental Lithospheric Mantle (DCLM) (after Nowell *et al.*, 2004). The figure presents a series of theoretical models for the evolution of the lithospheric mantle. Bold continuous lines represent the evolution of a melt residue formed by the removal of 10–20% equilibrium melt from a Bulk Silicate Earth (BSE) isotopic source in the presence of 10% residual pyrope garnet, and the complementary melt is shown as bold dotted lines ('melt evolution'). The evolution of some metasomitized peridotites (i.e. carbonate metasomatized, MARID or mica-rich compositions—Nowell *et al.*, 2004, and references therein) from an initial BSE isotopic composition over 1–1·5 Ga is shown by vectors 1–5. Bold dashed line represents the extent of samples in this study. Negative ε values can be modelled on the evolution of Archaean protoliths (Figs 7 and 8) whereas the large range of more positive ε_{Hf} values resembles the modelling of 3 Ga kimberlite-metasomatized DCLM (grey area) and can therefore be explained by extensive metasomatism of the Archaean protolith.

(Schulze *et al.*, 2003; Gonzaga *et al.*, 2009). The heterogeneity of O isotopes in eclogites compared with the relative homogeneity of O isotopes in garnet pyroxenites and mantle-derived clinopyroxenes (spinel- to garnet-facies mantle) is shown in Fig. 10 (Mattey *et al.*, 1994; Schulze *et al.*, 2003; Jacob, 2004; Gonzaga *et al.*, 2009). For garnet pyroxenites the relative homogeneity of Hf–Nd–Sr–O isotope compositions, similar to OIB, is consistent with a high-temperature 'magmatic' origin.

In contrast to the narrow range observed for mantle garnet pyroxenite xenoliths, Pearson *et al.* (1991) presented data for orogenic garnet pyroxenites from Beni Bousera that replicate the range of eclogite xenoliths, in contrast to the host peridotite, which shows mantle-like values. Some of these pyroxenites contain graphitized diamonds suggesting an origin in the eclogite facies (melted, subducted oceanic crust) followed by re-equilibration at lower temperatures, whereas others pyroxenites present evidence for high-pressure crystal fractionation processes. Pearson *et al.* (1991) argued that the Beni Bousera orogenic garnet clinopyroxenites were most likely to have crystallized from melts derived from hydrothermally altered oceanic lithosphere, although some garnet clinopyroxenites present evidence for formation from subducted oceanic crust following some partial melting. For the samples in this study, Gonzaga (2007) presented evidence of retrograde processes affecting xenoliths that were originally eclogites and now contain augitic clinopyroxene.

Unlike the orogenic garnet clinopyroxenites from Beni Bousera, Gonzaga (2007) suggested that the garnet clinopyroxenite xenoliths from this study are a result of interaction of a silica-rich melt with peridotite. Trace element data and K_D values calculated from garnet and clinopyroxene are identical to those from experimental data involving tholeiitic melts at mantle *P–T*, supporting a link to mantle-derived silicate melts for these xenoliths (Gonzaga *et al.*, 2009). Although the garnet pyroxenites may have similar elemental heterogeneity to eclogites, they are much younger and hence isotopically less heterogeneous. In contrast, the heterogeneity of Hf–Nd–Sr–O isotopes in

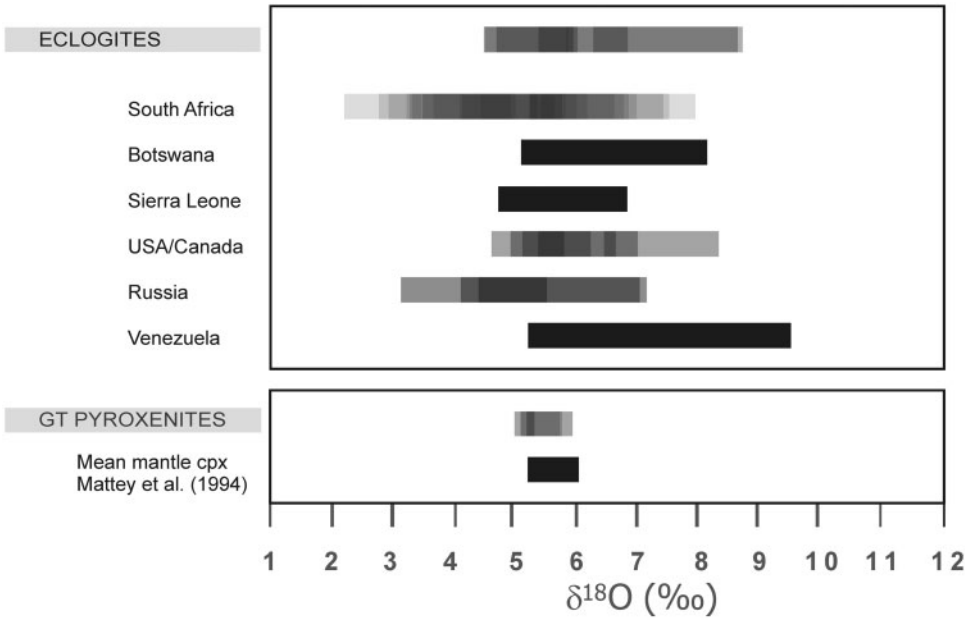

Fig. 10. Oxygen isotope data for clinopyroxenes and garnets from this study and from worldwide eclogites (after Gonzaga *et al.*, 2009, and references therein). Gradients in bars represent overlap of different data sources. The distinct oxygen isotope compositions suggest that garnet pyroxenite and eclogite xenoliths have distinct prehistories. Garnet pyroxenites overlap with 'mantle peridotite values' ($\delta^{18}O = 5{\cdot}5‰ \pm 0{\cdot}07$; Mattey *et al.*, 1994) supportive of a high-temperature origin fully equilibrated with mantle olivine. In contrast, the O isotope heterogeneity observed in eclogites is indicative of a complex history involving time and low as well as high temperatures.

cratonic eclogites reflects their antiquity and their complex evolution over 3 Ga.

CONCLUSIONS

(1) Lu–Hf clinopyroxene–garnet isochrons generally record older mantle events than Sm–Nd clinopyroxene–garnet isochrons by as much as *c.* 1000 Myr. However, in one eclogite (R30 from Roberts Victor) an Rb–Sr model age was considerably older than either the Lu–Hf or Sm–Nd model age.

(2) In some samples Sm–Nd and/or Lu–Hf mineral isochrons are reset by high-temperature (>1300°C) entrainment (e.g. in kimberlitic magma, Kaapvaal) or record the lower temperatures (<500°C) of emplacement in orogenic belts (e.g. during the Alpine Orogeny, Beni Bousera and the Himalayas).

(3) Rb–Sr, Lu–Hf and Sm–Nd data for eclogite R30 reveal the difficulty in relying upon any one isotope system to define the protolith age, as the range in 'ages' is 963–3105 Ma. Very unradiogenic clinopyroxenes (low Sm/Nd, low Rb/Sr and low Lu/Hf) may be a suitable proxy for protolith ages. Eclogite R30 defines an Archaean reservoir.

(4) Eclogites have extreme heterogeneous Hf–Nd–Sr isotope compositions overlapping with those of Kaapvaal metasomatized and unmetasomatized garnet- to spinel-facies mantle xenoliths and kimberlites and oceanic basaltic magmas (MORB and OIB). They also exhibit isotopic similarities to 'crustal' rocks.

(5) Group II megacrysts have similarities in Hf–Nd–Sr isotope compositions to eclogites and garnet pyroxenites, hinting at a similar petrogenesis. This may mean that the megacrysts could be disrupted eclogite protoliths or garnet pyroxenite veins.

ACKNOWLEDGEMENTS

We thank CAPES/Brazilian Government as the main sponsor of this research, and the Research Committee at the Department of Earth Sciences, Royal Holloway University of London for additional funding. Ian MacGregor is thanked for provision of the 'unique' Roberts Victor sample. We also would like to thank Professor G. Pearson, Dr M. Bizimis, Professor M. Wilson and an anonymous reviewer for their contributions.

FUNDING

This work was supported by the Brazilian Ministry of Education/Coordenação de Aperfeiçoamento de Pessoal de Nível Superior (CAPES) [BEX 1222-02-3] and the Research Committee at the Department of Earth Sciences, Royal Holloway, University of London.

REFERENCES

Anczkiewicz, R. & Thirlwall, M. F. (2003). Improving precision of Sm-Nd garnet dating by H_2SO_4 leaching — a simple solution to the phosphate inclusion problem. In: Vance, D., Müller, W. & Villa, I. M. (eds) *Geochronology: Linking the Isotopic Record with Petrology and Textures*. Geological Society, London: Special Publications, 220, 83–91.

Anczkiewicz, R., Platt, J. P., Thirlwall, M. F. & Wakabayashi, J. (2004). Franciscan subduction off to a slow start: Evidence from high precision Lu–Hf garnet ages on high grade blocks. *Earth and Planetary Science Letters* **225**, 147–161.

Becker, M. & LeRoex, A. (2006). Geochemistry of South African on- and off-craton, Group I and Group II kimberlites: petrogenesis and source region evolution. *Journal of Petrology* **47**, 673–703.

Bedini, R. M., Blichert-Toft, J., Boyet, M. & Albarède, F. (2002). Lu–Hf isotope geochemistry of garnet-peridotite xenoliths from the Kaapvaal craton and the thermal regime of the lithosphere. *Geochimica et Cosmochimica Acta* **66**(15A), A61.

Bedini, R. M., Blichert-Toft, J., Boyet, M. & Albarède, F. (2004). Isotopic constraints on the cooling of the continental lithosphere. *Earth and Planetary Science Letters* **223**, 99–111.

Birkhold-VanDyke, A. L., Neal, C. R., Jain, J. C., Mahoney, J. J. & Duncan, R. A. (1996). Multi-stage growth for the Ontong Java Plateau (OJP)? A progress report from San Cristobal (Makira), Solomon Islands. *EOS Transactions, American Geophysical Union* **77**, F714.

Bizimis, M., Sen, G., Salters, V. & Kesha, S. (2005). Hf–Nd–Sr isotope systematics of garnet pyroxenites from Salt Lake Crater, Oahu, Hawaii: Evidence for a depleted component in Hawaiian volcanism. *Geochimica et Cosmochimica Acta* **69**(10), 2629–2646.

Blichert-Toft, J. & Arndt, N. T. (1999). Hf isotope compositions of komatiites. *Earth and Planetary Science Letters* **171**, 439–451.

Blichert-Toft, J., Albarède, F., Rosing, M., Frei, R. & Bridgwater, D. (1999). The Nd and Hf isotopic evolution of the mantle through the Archean. Results from the Isua supracrustals, West Greenland, and from the Birimian terranes of West Africa. *Geochimica et Cosmochimica Acta* **63**(22), 3901–3914.

Cheng, H., King, L. R., Nakamura, E., Vervoort, J. D. & Zhou, Z. (2008). Coupled Lu–Hf and Sm–Nd geochronology constrains garnet growth in ultra-high-pressure eclogites from the Dabie orogen. *Journal of Metamorphic Geology* **26**(7), 741–758.

De Sigoyer, J., Chavagnac, V., Blichert-Toft, J., Villa, I. M., Luais, B., Guillot, S., Cosca, M. & Mascle, G. (2000). Dating the Indian continental subduction and collisional thickening in the northwest Himalaya: multichronology of the Tso Morari eclogites. *Geology* **28**, 487–490.

Gonzaga, R. G. (2007). Garnet–clinopyroxene assemblages in the Earth's mantle. PhD thesis, Royal Holloway University of London, 474 pp.

Gonzaga, R. G., Lowry, D., Jacob, D., LeRoex, A., Schulze, D. & Menzies, M. A. (2009). Eclogites and garnet pyroxenites—similarities and differences. *Journal of Volcanology and Geothermal Research* (John Gamble Symposium) (in press).

Hirschmann, M. M. & Stolper, E. M. (1996). A possible role for garnet pyroxenite in the origin of the 'garnet signature' in MORB. *Canadian Journal of Earth Sciences* **124**(2), 185–208.

Irving, A. J. (1980). Petrology and geochemistry of composite ultramafic xenoliths in alkalic basalts and implications for magmatic pocesses within the mantle. *American Journal of Science* **280**, 389–426.

Ishikawa, A., Kurirani, T., Makishima, A. & Nakamura, E. (2007). Ancient recycled crust beneath the Ontong Java Plateau; isotopic evidence from the garnet clinopyroxenite xenoliths, Malaita Solomon Islands. *Earth and Planetary Science Letters* **259**, 134–148.

Jacob, D. E. (2004). Nature and origin of eclogite xenoliths from kimberlites. *Lithos* **77**(1–4), 295–316.

Jacob, D. E., Bizimis, M. & Salters, V. J. M. (2002). Lu–Hf isotopic systematics of subducted ancient oceanic crust: Roberts Victor eclogites. *Geochimica et Cosmochimica Acta* **66**(16A), A360.

Jacob, D. E., Bizimis, M. & Salters, V. J. M. (2005). Lu–Hf and geochemical systematics of recycled ancient oceanic crust: evidence from Roberts Victor eclogites. *Contributions to Mineralogy and Petrology* **148**, 707–720.

Jagoutz, E., Dawson, J. B., Hoernes, S., Spettel, B. & Waenke, H. (1984). Anorthositic oceanic crust in the Archean Earth. *Proceedings of the 15th Lunar and Planetary Science Conference. Journal of Geophysical Research* **90**, Supplement, 395–396.

Kramers, J. D., Roddick, J. C. M. & Dawson, J. B. (1983). Trace element and isotope studies on veined, metasomatic and 'MARID' xenoliths from Bultfontein, South Africa. *Earth and Planetary Science Letters* **65**, 90–106.

Lapen, T. J., Medaris, L. G., Johnson, C. M. & Beard, B. L. (2005). Archean to Middle Proterozoic evolution of Baltica subcontinental lithosphere: evidence from combined Sm–Nd and Lu–Hf isotope analyses of the Sandvik ultramafic body, Norway. *Contributions to Mineralogy and Petrology* **150**, 131–145.

MacGregor, I. D. & Manton, W. I. (1986). Roberts Victor eclogites: ancient oceanic crust. *Journal of Geophysical Research* **91**, 14063–14079.

Mattey, D., Lowry, D. & Macpherson, C. (1994). Oxygen-isotope composition of mantle peridotite. *Earth and Planetary Science Letters* **128**(3–4), 231–241.

Nowell, G. M., Pearson, D. G., Bell, D. R., Carlson, R. W., Smith, C. B., Kempton, P. D. & Noble, S. R. (2004). Hf isotope systematics of kimberlites and their megacrysts: new constraints on their source regions. *Journal of Petrology* **45**(8), 1583–1612.

Pearson, D. G. & Nowell, G. M. (2004). Re–Os and Lu–Hf isotope constraints on the origin and age of pyroxenites from the Beni Bousera peridotite massif: implications for mixed peridotite–pyroxenite mantle sources. *Journal of Petrology* **45**(2), 439–455.

Pearson, D. G., Davies, G. R., Nixon, P. H., Greenwood, P. B. & Mattey, D. P. (1991). Oxygen isotope evidence for the origin of pyroxenites in the Beni Bousera peridotite massif, North Morocco: derivation from subducted oceanic lithosphere. *Earth and Planetary Science Letters* **102**, 289–301.

Pearson, D. G., Shirey, S. B., Carlson, R. W., Boyd, F. R., Pokhileno, N. P. & Shimizu, N. (1995). Re–Os, Sm–Nd and Rb–Sr isotope evidence for thick Archaen lithospheric mantle beneath the Siberian craton modified by multistage metasomatism. *Geochimica et Cosmochimica Acta* **59**(5), 959–977.

Poujol, M., Robb, L. J., Anhaeusser, C. R. & Gericke, B. (2003). A review of the geochronological constraints on the evolution of the Kaapvaal Craton, South Africa. *Precambrian Research* **127**, 181–213.

Scherer, E. E., Cameron, K. L. & Blichert-Toft, J. (2000). Lu–Hf garnet geochronology: Closure temperature relative to the Sm–Nd system and the effects of trace mineral inclusions. *Geochimica et Cosmochimica Acta* **64**(19), 3413–3432.

Scherer, E., Munker, C. & Mezger, K. (2001). Calibration of the lutetium–hafnium clock. *Science* **293**(5530), 683–687.

Schulze, D. J., Valley, J. W., Viljoen, K. S. F. & Spicuzza, M. J. (2003). Oxygen isotope composition of mantle eclogites. *8th International Kimberlite Conference Long Abstract*, pp. 1–2.

Shirey, S. B., Richardson, S. H. & Harris, J. W. (2004). Age, paragenesis and composition of diamonds and evolution of the

Precambrian mantle lithosphere of southern Africa. *South African Journal of Geology* **107**(1–2), 91–106.

Simon, N. S. C., Carlson, R. W., Pearson, D. G. & Davies, G. R. (2002). The Lu–Hf isotope composition of cratonic lithosphere: disequilibrium between garnet and clinopyroxene in kimberlite xenoliths. *Goldschmidt Conference Abstracts* **66**, A717.

Simon, N. S. C., Carlson, R. W. & Graham, D. (2007). The origin and evolution of the Kaapvaal cratonic lithospheric mantle. *Journal of Petrology* **48**(3), 589–625.

Smith, C. B. (1983). Pb–Sr and Nd isotopic evidence for sources of southern African Cretaceous kimberlites. *Nature* **304**, 51–54.

Sobolev, A. V., Hofmann, A. W., Sobolev, S. V. & Nikogosian, I. K. (2005). An olivine-free mantle source of Hawaiian shield basalts. *Nature* **434**(7033), 590–597.

Soderlund, U., Patchett, J. P., Vervoort, J. D. & Isachsen, C. E. (2004). The Lu-176 decay constant determined by Lu–Hf and U–Pb isotope systematics of Precambrian mafic intrusions. *Earth and Planetary Science Letters* **219**(3–4), 311–324.

Stevenson, R. K., Bizzarro, M., Simonetti, A. & Gariepy, C. (2002). Hf isotope composition of 3 Ga komatiites from Ontario, Canada. *Geochimica et Cosmochimica Acta* **66**(15A), A741.

Tejada, M. L. G., Mahoney, J. J., Neal, C. R., Duncan, R. A. & Petterson, M. G. (2002). Basement geochemistry and geochronology of Central Malaita, Solomon Islands, with implications for the origin and evolution of the Ontong Java Plateau. *Journal of Petrology* **43**(3), 449–484.

Thirlwall, M. F. (1991). Long-term reproducibility of multicollector Sr and Nd isotope ratio analysis. *Chemical Geology* **94**, 85–104.

Thirlwall, M. F. & Anczkiewicz, R. (2004). Multidynamic isotope ratio analysis using MC-ICP-MS and the causes of secular drift in Hf, Nd and Pb isotope ratios. *International Journal of Mass Spectrometry* **235**, 59–81.

Titterington, D. M. & Halliday, A. N. (1979). On the fitting of parallel isochrons and the method of maximum likelihood. *Chemical Geology* **26**, 183–195.

Vance, D. & Thirlwall, M. F. (2002). An assessment of mass discrimination in MC-ICPMS using Nd isotopes. *Chemical Geology* **185**, 227–240.

Workman, R. K. & Hart, S. R. (2005). Major and trace element composition of the depleted MORB mantle (DMM). *Earth and Planetary Science Letter* **231**, 53–72.

York, D. (1969). Least-squares fitting of a straight line with correlated errors. *Earth and Planetary Science Letters* **5**, 320–324.